

AN ABSTRACT OF THE THESIS OF

Caitlin P. Forinash for the degree of Master of Science in Mechanical Engineering
presented on June 8, 2016.

Title: Floating Offshore Wind Array Systems Optimization off the US West Coast
using an Extended Pattern Search Algorithm

Abstract approved:

Bryony L. DuPont

The large wind resource off the United States West Coast has the potential to generate wind power for millions of homes, yet the high cost of energy for offshore wind power compared to traditional sources has slowed the development of offshore wind farms in the US. The four studies presented in this work explore optimal layouts for floating offshore wind energy systems off the US west coast in order to drive down costs. A moderately stochastic optimization method known as an Extended Pattern Search (EPS) is applied to a unidirectional, single wind speed case, and a multidirectional, multiple wind speed case. Another study is presented that evaluates commonly-implemented and symmetrical wind farm layouts in both unidirectional and multidirectional wind cases. Lastly, a study is presented that explores the use of seeded initial layouts in the optimization of wind energy systems.

Three advanced models are incorporated into the EPS: (1) a cost model developed specifically for this work, (2) a power development model that selects hub height and rotor radius to optimize power production, and (3) a wake propagation and interaction model that determines aerodynamic effects. Results from this work derive best practices that can be employed by offshore wind farm developers to improve the layout of platforms, and may contribute to reducing barriers to implementation, enabling developers and policy makers to have a clearer understanding of the resulting cost and power production of computationally optimized farms.

©Copyright by Caitlin P. Forinash
June 8, 2016
All Rights Reserved

Floating Offshore Wind Array Systems Optimization off the US West Coast using an
Extended Pattern Search Algorithm

by
Caitlin P. Forinash

A THESIS

submitted to

Oregon State University

in partial fulfillment of
the requirements for the
degree of

Master of Science

Presented June 8, 2016
Commencement June 2016

Master of Science thesis of Caitlin P. Forinash presented on June 8, 2016

APPROVED:

Major Professor, representing Mechanical Engineering

Head of the School of Mechanical, Industrial, and Manufacturing Engineering

Dean of the Graduate School

I understand that my thesis will become part of the permanent collection of Oregon State University libraries. My signature below authorizes release of my thesis to any reader upon request.

Caitlin P. Forinash, Author

ACKNOWLEDGEMENTS

To Heather Dillon, for encouraging me to pursue a higher education and believing in my abilities as a student, researcher, and person.

To Belinda Batten and Bob Paasch, for welcoming me into NNMREC and giving me the opportunity to explore the realm of marine renewable energy.

To Kyle Niemeyer, for providing me with immense support and, without whom, I would not have completed my research.

To Mom and Dad, for giving me endless hope and love, and for always offering help.

And to Bryony, who has been the most incredible, supportive, and entertaining advisor I could have asked for. Thank you for going on this journey with me.

TABLE OF CONTENTS

	<u>Page</u>
Chapter 1: Introduction	1
Chapter 2: Previous Approaches	3
2.1 Wind Farm Optimization	3
2.1.1 Onshore Wind Farm Optimization	3
2.1.2 Offshore Wind Farm Optimization.....	4
2.2 Pattern Search Optimization.....	5
2.3 Extended Pattern Search Optimization	6
2.4 Offshore Wind Farm Models	7
2.4.1 Cost Modeling.....	7
2.4.2 Wake and Power Modeling	10
Chapter 3: Modeling	15
3.1 Power Model	15
3.1.1 Turbine Geometry Selection	15
3.2 Wake Propagation and Interaction Model.....	16
3.3 Cost Model.....	18
3.3.1 Turbine and Platform Capital Cost.....	19
3.3.2 Cabling Cost.....	19
3.3.3 Anchoring and Mooring Cost	20
3.3.4 Annual Operations and Maintenance Cost.....	21
3.3.5 Substation Cost	21
3.3.6 Installation Cost	22
3.3.7 Leasing Cost.....	22
3.3.8 Other Cost Considerations.....	23
3.3.9 Onshore Cost Model.....	23
Chapter 4: Extended Pattern Search Approach	24
4.1 Introduction.....	24
4.2 Pattern Search.....	26
4.3 Stochastic Extensions	26
4.3.1 Randomized Initial Layout.....	26

TABLE OF CONTENTS (Continued)

	<u>Page</u>
4.3.2 Randomized Search Order.....	27
4.3.3 Popping.....	27
4.4 Objective Function.....	27
4.5 Stopping Criteria.....	28
Chapter 5: Problem Formulation.....	29
5.1 Unidirectional Wind Case.....	29
5.2 Multidirectional Wind Case	31
5.3 Hard-Coded Layout Study.....	32
5.4 Seeded Initial Layout Study	33
Chapter 6: Unidirectional Wind Case Results and Discussion	36
6.1 Results.....	36
6.2 Discussion	40
Chapter 7: Multidirectional Wind Case Results and Discussion	43
7.1 Results.....	43
7.2 Discussion	46
Chapter 8: Hard-Coded Layout Study Results and Discussion	48
8.1 Results.....	48
8.2 Discussion	48
Chapter 9: Seeded Initial Layout Study Results and Discussion	50
9.1 Results.....	50
9.2 Discussion	54
Chapter 10: Conclusions	56
Chapter 11: Future Work	59
11.1 Additional Studies.....	59
11.2 Co-Located Array Optimization	60
11.3 Optimizing Cabling	60
References.....	61

LIST OF FIGURES

<u>Figure</u>	<u>Page</u>
Fig. 1: Generic wind turbine power curve	11
Fig. 2: Three dimensional wake propagation	17
Fig. 3: Wind speed in a wake downstream of a rotor	18
Fig. 4: Multiple wakes interacting with a rotor swept area	18
Fig. 5: EPS Pseudocode	25
Fig. 6: Unidirectional wind case	29
Fig. 7: Wind onset angle and fraction of occurrence for multidirectional, multiple speed wind case	31
Fig. 8: Empirically-derived wind farm layouts	33
Fig. 9: Initial layout for a wind farm with side lengths of 4000 m	34
Fig. 10: Initial layout for a wind farm with side lengths of 2000 m	35
Fig. 11: Objective evaluation for offshore layouts containing 15 to 60 turbines	36
Fig. 12: Objective evaluation for onshore layouts containing 15 to 60 turbines	37
Fig. 13: Turbine geometry key	37
Fig. 14: 42-turbine offshore layout, objective evaluation = $-1.79456e+08$	37
Fig. 15: 32-turbine onshore layout, objective evaluation = $-1.64933e+08$	38
Fig. 16: 16-turbine layout, EPS, 100% efficiency	39
Fig. 17: 16-turbine layout, Adapted GA, 100% efficiency (Liu and Wang [29])	39
Fig. 18: Efficiency of EPS-generated layouts	40
Fig. 19: 34-turbine layout, EPS, 100% efficiency	40
Fig. 20: Objective Evaluation for layouts containing one to 22 turbines	43
Fig. 21: Turbine geometry key	44
Fig. 22: Optimized layout containing five turbines, objective evaluation = $\$9.93 \times 10^6$	44

LIST OF FIGURES (Continued)

<u>Figure</u>	<u>Page</u>
Fig. 23: Optimized layout containing seven turbines, objective evaluation = - \$1.20x10 ⁷	45
Fig. 24: Optimized layout containing 12 turbines, objective evaluation = -\$8.96x10 ⁶	45
Fig. 25: Objective evaluations for 4000 meter optimized farms containing 16-52 turbines, seeded initial layouts	50
Fig. 26: Objective evaluations for 4000 meter optimized farms containing 16-52 turbines, random initial layouts	51
Fig. 27: Objective evaluations for 2000 meter optimized farms containing 4 – 48 turbines, seeded initial layouts	52
Fig. 28: Objective evaluations for 2000 meter optimized farms containing 4 – 48 turbines, random initial layouts	52
Fig. 29: 44 turbine, 4000 meter layout from seeded initial layout case; objective evaluation = -\$1.74E+08.....	53
Fig. 30: 20 turbines, 2000 meter layout from seeded initial layout case; objective evaluation = -\$5.25E+07.....	54
Fig. 31: Wind rose with wind speeds and percentage of occurrence at each wind direction.	59
Fig 32: Seeded initial layout for multidirectional, multiple wind speed case.	60

LIST OF TABLES

<u>Table</u>	<u>Page</u>
Table 1: Offshore and onshore wind farm parameters	30
Table 2: EPS and Adapted GA comparison parameters	31
Table 3: Offshore environment characteristics	32
Table 4: Minimum objective evaluations for offshore and onshore layouts	38
Table 5: Objective Evaluation and AEP Results for Layouts 1-9, Cases 1 and 2.....	48

Chapter 1: Introduction

As population continues to grow and Americans increasingly use technological and powered products, it is predicted that the demand for power in the United States will increase by as much as 29% by the year 2040 [1]. Meeting this need will require not only the advancement of existing renewable energy systems (such as onshore wind farms and solar arrays), but also the development of novel renewable energy systems.

Wind power is the fastest growing electricity source in the US and Europe [2]. In recent years, much of the European wind power expansion has been offshore wind power installations. By the end of June 2015, a total of 82 wind farms in 11 European countries were fully grid connected for a total of 10,394 MW of installed offshore wind power [3]. While the US does not yet have any installed offshore wind farms, the United States Department of Energy (DOE) estimates that approximately 54 MW of offshore wind power will be installed off the coasts of the U.S. by 2030 [4]. While many proposed farms are to be located in the shallower waters off the northeast and mid-Atlantic states, it is imperative to capitalize on the large wind resource off the deep-water west coast of the United States, whose predicted resource totals more than 900 GW [5].

The vast majority of offshore wind projects have been embedded wind farms that use either bottom-fixed monopoles, jackets, or gravity-based foundations to support wind turbines [6]. These embedded structures are best used for water depths ranging from 10 to 15 meters [7], although the costs do not become prohibitive until a water depth of 30 meters [8]. Extra-long (XL) monopoles may be feasible in water depths up to 40 meters, and deep-water jackets can support turbines in water depths of 30-60 meters [9]. The waters off the coasts of leading European countries, as well as the North American east coast, lend themselves well to these types of turbines since the waters are shallow and the bathymetry is gentle. However, the North American west coast has a sharper bathymetry, making the use of embedded offshore wind turbines impractical.

Expanding offshore wind technologies into deeper water increases the resource area as well as the total available wind resource, since wind speeds are higher and more predictable over deep waters [10]. Since embedded platforms are not possible in deep

ocean waters, other options must be considered. There are many proposed floating platform designs; three current platform designs are spar-buoy, tension leg-platform (TLP), and semi-submersible. HyWind is the first full-scale floating turbine; it is located off the coast of Norway in 200-meter water depth and has been grid-integrated since 2010. It is a spar-buoy, long-ballast column design. Another floating wind turbine, the WindFloat semi-submersible platform designed by the US company Principle Power, has a 2 MW project located 5 kilometers off the coast of Portugal [11]. It has been generating electricity since 2012 and has produced nearly 10 million kWh since its implementation. An additional three or four 6-8 MW floating turbines are to be installed by 2017 at the Portugal site [12].

The US west coast has made progress in recent years with Oregon leading the industry in offshore wind development. According to the National Renewable Energy Laboratory, at 12 miles off the Oregon Coast there is a potential wind resource of nearly 220 GW [13]. As of May 2014, a new project has been commissioned by the DOE, WindFloat Pacific, which will develop 30 MW of wind power in deep waters off the coast of Coos Bay, Oregon [14].

The high cost of offshore wind farms can be prohibitive; in addition, structures in water have many inherent complications. Offshore turbines are often difficult to maintain due to extreme weather conditions; if a turbine were to malfunction during a stormy duration of the year it could be many weeks before a team could access the site to fix it. There are also higher installation and maintenance costs for offshore turbines, although it is expected that the higher resources and dispatchability of the wind energy potential can compensate these costs. For the offshore wind industry to thrive, research must be conducted that will help lower the costs of offshore wind power installations. Optimizing the layouts such that power production is maximized and cost is minimized will help make offshore wind power installations more feasible and affordable.

Chapter 2: Previous Approaches

2.1 Wind Farm Optimization

Optimizing an offshore wind farm requires the consideration of many factors such as turbine placement, cabling, installation, and operations and maintenance costs (O&M). For floating wind farms, mooring and wave effects also must be considered. Researchers typically use one of two common objectives when optimizing wind farms: maximizing the Annual Energy Production (AEP), or minimizing the Cost of Energy (COE). Maximizing AEP is achieved by placing turbines such that wake effects are minimized, and maximizing the size of wind turbines in order to capture more energy. However, minimizing COE may require reducing the size or number of wind turbines in a farm. These objectives are interrelated: while a farm's design may cause AEP to increase, the initial and annual costs may increase even more, which in turn raises the COE. Due to this relationship between AEP and COE, reducing the cost of wind power may require sacrificing some energy production.

Early wind farm optimization considered primarily onshore wind farms; however, as offshore wind technologies have developed, more research is being conducted in optimizing bottom-fixed and floating offshore wind farms.

2.1.1 Onshore Wind Farm Optimization

Onshore wind farm optimization has been extensively researched using different techniques and objective functions. Mosetti et al. [15] developed a Genetic Algorithm (GA) to maximize energy production while minimizing cost; this work has since been expanded and improved for more wind farm applications. The work described in this document explores the application of an Extended Pattern Search (EPS) algorithm to offshore wind farm layout optimization while expressly considering the challenges of deep-water installations. Research using the EPS has shown to significantly improve the performance of onshore wind farms, using both profit and COE objectives [16–19]. Other onshore wind farm optimization methods include a Greedy Improvement Heuristic methodology to determine wind turbine placement used by Ozturk et al. [20], and Particle Swarm Optimization (PSO) methods used by Wan et al. [21] and

Pookpupnt et al. [22]. While there are clear pros and cons of each of these methods (particularly in terms of layout optimality, computational expense, and models applied) they have all been successful in generating theoretical onshore wind farm layouts.

2.1.2 Offshore Wind Farm Optimization

Offshore wind farm optimization literature has generally concentrated on bottom-fixed wind farms. Commonly, optimization methods focus on maximizing power output and efficiency of wind farms, with some methods minimizing cost as well. Elkinton et al. developed models that can be applied to any heuristic optimization algorithm for offshore wind farms that maximize power and minimize cost [23,24]. An objective function that minimizes the Levelized Cost of Energy (LCOE) was used, and it was found that Genetic Algorithms (GA) and Greedy Heuristic Algorithms were the most viable optimization methods for the offshore wind farm layout problem; however, the models were not applied within an Extended Pattern Search (EPS) method. Pérez et al. also developed a method that can be applied to any heuristic: a two-step sequential procedure combines a heuristic method to set a random initial layout with nonlinear mathematical program techniques that search the space to find local optima [25]. This method was applied to the Alpha Ventus offshore wind farm and, compared to the actual layout, increased the Annual Energy Production (AEP) by 3.76%.

Genetic Algorithms (GAs) have been the most common method for offshore wind farm layout optimization. These methods are highly stochastic, which increases convergence to good solutions in multi-modal systems such as the offshore wind farm layout problem. However, GA's generally require the placement of turbines in discrete locations, which limits possible layout combinations. For aligned, staggered, and scattered layout optimization, Gao et al. found that scattered layouts optimized using a Multi-Population GA resulted in the most optimal AEP [26,27]. A model developed by Réthoré et al. included electrical grid and foundation costs as well as energy production [28]. The multi-fidelity model approach that combined 1000 iterations of a Simple GA with 20 iterations of a Sequential Linear Programming method was applied to a case at Middelgrunden Wind Farm in Denmark and was found to limit the computational cost of optimization [28]. Liu and Wang developed an Adapted GA method that replaces

the location swaps of traditional GA's with random crossovers; a wind farm containing 16 turbines in a unidirectional, single wind speed case was optimized to 100% efficiency using this method [29].

Additional heuristic optimization methods for multi-modal spaces have been applied to the offshore wind farm layout problem. Rivas et al. developed a Simulated Annealing Algorithm that employed three local search operations; their algorithm increased the AEP of the Horns Rev offshore wind farm by 1% [30]. Using a Coral Reefs Optimization Algorithm, Salcedo-Sanz et al. improved offshore wind farm performance over meta-heuristic algorithms, including Evolutionary Algorithms, Differential Evolution, and Harmony Search [31]. A Viral Based Algorithm with an objective function based on Cost of Energy (COE) was developed by Ituarte et al. that decreased COE for a 30-turbine farm, as compared to the layout of Mosetti et al.'s GA approach [32].

Rodrigues et al. developed a Covariance Matrix Adaptation Evolutionary Strategy (CMA-ES) in a nested configuration to optimize the layout of a floating offshore wind farm comprised of IDEOL platforms supporting 5 MW turbines [33,34]. This method can optimize layouts in a continuous space for both stationary and moveable platforms. Results from the stationary case showed a decrease in Levelized Production Cost (LPC) of -4.17% over a non-optimized grid layout.

2.2 Pattern Search Optimization

Pattern search algorithms are deterministic methods for optimization that search a space in a pattern of directions without the use of derivatives. Torczon introduced a class of pattern search methods for optimizing unconstrained nonlinear problems by combining direct search methods [35]. Torczon and Trosset found that, while simplex methods can be unreliable, pattern searches guarantee convergence to a stationary point and can be used when derivatives are unavailable and the objective function is not smooth [36].

Aladahalli et al. introduced a metric for geometric layouts called the sensitivity metric [37]. The sensitivity metric estimates the effect of pattern moves on the objective

function, and schedules patterns in decreasing order of their effect on the objective function to increase efficiency. Yin and Cagan explored the effectiveness of different heuristics for generating pattern directions to be used in the pattern search to compare against the coordinate search method [38]. The four methods – conjugate, modified gradient method, rank ordering method, and simplex method – did not significantly improve results but did increase complexity over the coordinate search method.

Vaz and Vicente combined a stochastic particle swarm scheme to increase global convergence with a deterministic pattern search [39]. The pattern search is able to find local minima, while the particle swarm heuristic explores the possible nonconvexity of the objective to improve global convergence. Cagan presented 3D component layout optimization methods for nonlinear and multimodal spaces, which deterministic algorithms are unable to navigate [40]. Heuristic rule-based approaches are also not suitable for nonlinear, non-differentiable functions. Therefore, a balance between deterministic and stochastic methods must be found, such as in the EPS, which combines the deterministic pattern search with stochastic extensions to increase convergence to good solutions [40].

2.3 Extended Pattern Search Optimization

An Extended Pattern Search (EPS) is a moderately stochastic non-gradient search method that traverses the search space in a series of user-defined moves. The EPS combines a deterministic pattern search algorithm with stochastic extensions. This work uses three extensions that will be explained in further detail: randomized initial layout, randomized search order, and a popping algorithm. The added stochasticity allows for the EPS to avoid settling on local optima. Another benefit of EPS methods is that they enable the inclusion of advanced modeling as new technologies for offshore wind farms are introduced. Modeling advances must be incorporated into the EPS to account for the challenges of deep-water installations. These modeling advances include cost, power development, and wake propagation and interaction models.

DuPont et al. successfully applied Extended Pattern Search methods to onshore wind farm layout and turbine geometry optimization [16–19]. The EPS is a moderately stochastic method well-suited for large, multi-modal systems such as the offshore

floating wind farm layout and turbine geometry optimization problem. The profit objective used in previous work [16,18,19] informs developers of approximate costs and power production of wind farms, and allows for the inclusion of new models such as a cost model that considers the high costs of offshore floating wind farms comprised of WindFloat floating platforms [11].

2.4 Offshore Wind Farm Models

In order to optimize floating offshore wind farms, analytical models must be used that mathematically define the problem being solved. Floating offshore wind systems optimization is a complex problem with many factors, therefore applying models that closely represent the problem are computationally expensive. This section describes cost, power, and wake models that have been applied to wind farm optimization in previous work.

2.4.1 Cost Modeling

Mosetti et al. [15] developed a cost model that has been used in many early onshore wind farm optimization studies [20][22][41]. In the cost model, the cost per year for a single turbine is non-dimensionalized to a value of 1, and the equation used to solve for the total cost of a wind farm is given as:

$$C_{\text{tot}}(N) = N\left(\frac{2}{3} + \frac{1}{3}e^{-0.00174N^2}\right) \quad (1)$$

where N is the number of turbines in the farm. The limit of the total cost approaches $\frac{2}{3}N$ when $N > 50$, where the cost of each turbine installed on the farm is two-thirds of the cost of a single installation. Liu et al. applies Mosetti's method for the cost function of an offshore wind farm [29]. Rivas et al. applies Mosetti's model as a part of an objective formulation and assumes that, in most cases, as annual energy production (AEP) is maximized, the profit is also maximized [30]. A simple cost model is used by Salcedo-Sanz et al.; in this model, the cost of the wind farm is equal to the total cost of a single

installation multiplied by the number of turbines [31]. However, other cost models have been specifically developed for offshore wind farm applications. Costs are expected to be higher offshore due to additional components and operations and maintenance (O&M), as well as the use of specialty equipment.

Elkinton et al. [42] estimates the levelized production cost (LPC) for onshore wind farms using the equation:

$$LPC = \frac{C_{inv}}{a.E_a} + \frac{C_{O\&M}}{E_a} \quad (2)$$

where C_{inv} is the total investment cost, $C_{O\&M}$ is the annual O&M cost, a is the annuity factor, and E_a is the annual energy production of the farm. Gao et al. [26] has broken up cost into 5 parts: 33% of the total cost is attributed to capital costs, 23% is attributed to O&M costs, 24% is attributed to support structure costs (assuming an embedded or gravity-based structure), 15% is attributed to grid connection costs, and 5% is attributed to other miscellaneous costs. The levelized cost of energy (LCOE) can be calculated using the equation:

$$LCOE = (C_c \times FCR + C_{O\&M}) / APG \quad (3)$$

where C_c are the construction costs, $C_{O\&M}$ are the O&M costs, FCR is the fixed charge rate assumed to be 15%, and APG is the annual power generation.

R  thor   et al. used a cost model that only includes costs relevant to the optimization [28]. This many-part optimization model uses the object cost function:

$$WP_n = WP - CD - CM \quad (4)$$

where WP_n is the net value of the power production, WP is the value of the wind farm power production over the lifetime, CD is the accumulated components degradation, and CM is the cost of overall maintenance. The financial cost:

$$C = CF + CG \quad (5)$$

where CF are the foundation costs, and CG are the electrical and infrastructure costs. WP_n and C are then applied to the financial balance equation:

$$FB = WP_n - C \left(1 + \left(\frac{r_{cl} - r_i}{N_L}\right)\right)^{XN_L} \quad (6)$$

where r_{cl} is the interest rate that the wind farm consortium has to pay for loans, r_i is the rate of inflation, X is the wind farm life in years, and N_L is the number of times interest of loans must be paid per year.

Capital costs for offshore wind projects are higher than onshore due to the challenging installation environment and additional components, such as embedded monopiles, deep-water jackets, floating platforms, offshore transmission cabling, and substations. Fuglsang et al. calculated that the component weight for offshore embedded wind installations is 42% higher than onshore due to grid connections and foundation [43]. However, Fuglsang et al. also states that there is an annual energy production increase from onshore to offshore of 28%. For floating installations, the balance of system (BOS), or floating platform, adds significantly to the cost. According to Butterfield et al., if the cost of a platform can be held at 25% of the total capital cost, then a cost of energy of \$0.05/kWh is achievable, making floating offshore wind farms affordable [44].

The cost of transmission cabling used to transport the electricity from offshore wind farms to shore adds significantly to the total cost of offshore wind power projects. According to Breseti et al., the average cost of offshore transmission cable installations are \$55,290/km [45]. The project-specific costs depend on voltage level, laying technology, presence of existing infrastructures, and requirements of mechanical

protection [45]. Maintenance costs for the cabling are approximately \$221,160/year [45]. Over the 20 year life of a wind farm, each connection is expected to fail an average of one time with a mean time of 30 days to repair [45]. Mooring and anchoring costs are also substantial; Castro-Santos et al. identified four parts of the total mooring and anchoring system costs [46]:

$$C_{ma} = C3_{ma} + C4_{ma} + C5_{ma} + C6_{ma} \quad (7)$$

these represent the manufacturing ($C3_{ma}$), installation ($C4_{ma}$), exploitation ($C5_{ma}$), and dismantling costs ($C6_{ma}$).

Operations and maintenance (O&M) account for the majority of annual expenses. Maintenance depends on cooperative weather windows and special vessels that can add to both the difficulty and the cost of maintaining the farm. According to Bussel et al., more than 50% of average yearly O&M costs are for lifting operations that require special equipment [47]. According to Butterfield et al., due to the cost of these vessels, long-term maintenance may be easier and most cost-effective onshore at a dry dock [44]. This is most relevant for tuggable, stable platforms such as the WindFloat [11]. However, dry-dock maintenance would not be as feasible for a spar buoy platform such as HyWind [48]. According to Henderson et al., towing is susceptible to malfunction, therefore onsite maintenance is preferable for nearly all failure mechanisms [49]. Bussel et al. estimated that yearly O&M costs account for 4-4.5% of total investments [47]. Henderson et al. gave a less conservative estimate of 2.2% [49]. Farm-like designs can help to reduce some of the major maintenance costs; given the high cost of O&M, optimization of O&M methods will be necessary to help reduce the cost of offshore wind in the future [47].

2.4.2 Wake and Power Modeling

Wind turbines generate power by converting the power in the wind into electricity. Three stages of wind power generation are defined (Fig. 1): (1) wind speed is below the wind turbine's cut-in wind speed or above the cut-out wind speed and no power is

produced; (2) the wind speed is between the wind turbine's cut-in and rated wind speed, and power is produced with a cubic relationship to the wind speed; and (3) the wind speed is between the wind turbine's rated and cut-out wind speed, and power is produced at the wind turbine's rated, or maximum power.

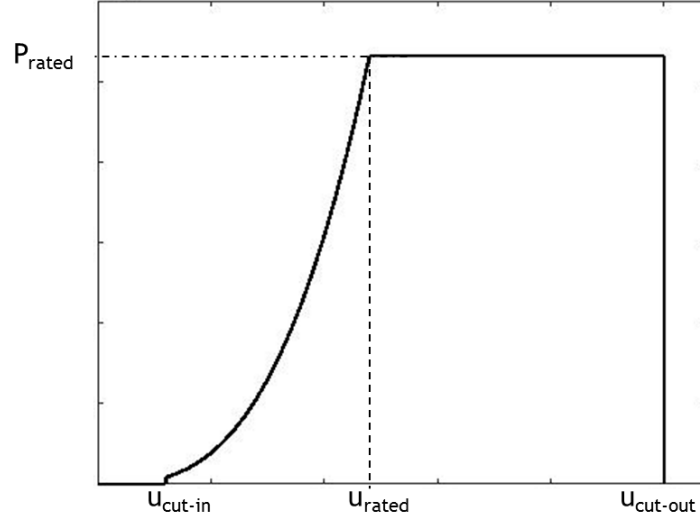


Fig. 1: Generic wind turbine power curve

The wind turbine power equation is defined as:

$$P(u) = \begin{cases} 0, & u < u_{cut-in} \\ \frac{1}{2}\rho A C_p u^3, & u_{cut-in} \leq u \leq u_{rated} \\ P_{rated}, & u_{cut-out} > u > u_{rated} \end{cases} \quad (8)$$

where P is power, ρ is the density of air (measured at the turbine's nacelle), A is the swept area of the rotor, C_p is the coefficient of power, u is the wind speed, P_{rated} is the rated power of the turbine, u_{cut-in} is the cut-in wind speed, u_{rated} is the rated wind speed, and $u_{cut-out}$ is the cut-out wind speed. As there is a cubic relationship between effective wind speed and resulting power development, small changes in wind speed can cause large changes in power generation. When multiple turbines are placed close enough to have aerodynamic interaction, wakes created behind the rotor of each turbine affect the wind speed and affect turbulent air flow. Therefore, in order to understand power development and determine how power is developed in a wind farm, wake effects must be studied.

Wind speeds and directions vary based on location, terrain, time of year, and even time of day; many models have been developed to calculate and predict wind speeds over the area of a wind farm. The Weibull Distribution is a probability density function that is widely used in the wind energy industry to describe the wind speed [30]. A linearized model, Wind Atlas Analysis and Application Program (WAsP) is an industry-standard software package that can be used for siting wind farms on complex terrain [50]. WAsP generates a local wind climate based on meteorological data from a measurement station and accounts for surface roughness, complex terrain, and obstacles [51]. Kusiak et al. presented two prediction methods: a direct prediction model and an integrated prediction model [52]. The direct prediction model directly predicts the power of the field from weather forecasting data, while the integrated prediction model predicts the wind speed from weather data with a power prediction from the wind speed [52]. The direct prediction model predicts performance better than the integrated prediction model. Long-term wind speed prediction is helpful for operation management of the wind energy market, whereas short-term prediction models are more useful for on-site management of a wind farm [52]. Prediction models such as these can be implemented as advanced models into optimization framework to more accurately predict power production and profit of floating offshore wind farms.

In order to predict the power produced by a wind farm, as well as to optimize the placement of wind turbines within an array, aerodynamic interactions between wind turbines must be well-understood. Many wake models have been developed in order to model these aerodynamic interactions, allowing developers to more effectively predict power generation within a wind farm prior to installation. Jensen developed an early wake model in 1983; this simplified model describes the wake behind a single wind generator [53]. The model can be used to estimate the power production from multiple turbines in close proximity by determining the wind speed downstream of a turbine. Jensen's model has been used and modified for many applications [26,33,42,54,55]. Another commonly used wake model was developed by Ainslie in 1988 [56]. This model has been used by many researchers to determine power development in wind farms [50,51,57–59]. Ainslie's model includes the influence of meteorological

conditions on wake decay. This model has good agreement with wind tunnel studies and field data [56].

Jensen and Ainslie's low-fidelity wake models are simple and reduce computational time compared to higher-fidelity models [53], [56]. However, low-fidelity models often over-predict power generation [50]. Kusiak et al. described a method for determining wake effects at a given turbine on an offshore wind farm [60]. In this model, the wake expands linearly behind the rotor and the free stream speed is reduced [60]. Sørensen et al. used both a diversified model that represents each turbine individually and an aggregation that represents the entire wind farm by a single turbine [61].

The Dynamic Wake Meandering (DWM) model is a medium-fidelity model that describes the downstream advection of a wake from a turbine [62]. Réthoré et al. combined a DWM model with the wind turbine simulation tool HAWC2 [28]. Salcedo-Sanz calculated wakes and production estimation using freely-available Openwind software [31]. Other software include Farm Layout Program (FLaP), WAKEFARM from Energy Research Centre of the Netherlands (ECN), and CRES-flowNS [51,58], [63]. FLaP is an axisymmetric wake model that estimates wind speed at any point in a wind farm and has been advanced to further describe wake development offshore [58]. WAKEFARM is based on parabolized Navier-Stokes, and CRES-flowNS uses pressure field corrections [51].

Many Computational Fluid Dynamics (CFD) models have been developed to describe the velocity field for single turbines, and more recently, entire wind farms. CFD wake models are high-fidelity tools that can be computationally expensive. The highest-fidelity models are large eddy simulation (LES) models that can take several weeks to complete [33]. Some of these CFD models include the eddy viscosity wake model in GH WindFarmer [51], CENER based on Fluent [51], NTUA [51], Simulator for Offshore Wind Farm Applications (SOWFA) by NREL [33], EllipSys3D by DTU and Risoe [33], and FarmFlow by ECN [64,65]. Martínez developed an elliptic model based on the actuator disk technique to improve the accuracy of CFD output variables using OpenFoam, an open source CFD solver, adapted for onshore and offshore sites

[66]. As mentioned previously, while low-fidelity models often over-predict power production, CFD models often under-predict power generation [50].

Rodrigues et al. modeled wake effects more specifically for the application of moveable floating wind turbines on IDEOL platforms [33],[34]. The IDEOL foundations have two degrees of freedom and are controlled such that their wakes are not fixed with wind direction [34]. Two models are used: the Jensen model during the optimization routine [53], and FarmFlow to verify efficiency [64]. FarmFlow is an improved version of the UPMWAKE model which solves the Navier-Stokes equations in all three dimensions [64].

Due to variations between wind and wake characteristics over land versus water, models must either be modified or developed for offshore environments in order to accurately predict wake effects offshore [67]. Surface roughness over the sea surface is 0.0002 m, which is much smoother than over land which has a surface roughness of 0.03 m [68]. In addition, turbulence caused by mechanical processes, such as the rotation of turbine blades, is much smaller offshore [67]. Therefore, the influence of sensible and latent heat fluxes on turbulence is much more significant offshore [67]. Sea surface temperature is more consistent over the course of the day but has very pronounced seasonal differences compared to onshore, which also affects wind conditions [67].

Hegberg conducted a 1:400 scale experiment to test wind wakes [69]. The turbines used had 25 cm hub heights and were 2-bladed to more accurately create wind turbine wake characteristics. The study concluded that wind farm models are not sufficiently accurate and often over-predict production.

Chapter 3: Modeling

3.1 Power Model

Power is produced by individual turbines based on the turbine's power curve; turbines of different sizes have different power curves (Fig. 1). Each turbine model has a cut-in wind speed, rated wind speed, and cut-out wind speed. At wind speeds below the cut-in wind speed, the turbine does not produce power. At wind speeds above the rated wind speed and below the cut-out wind speed, the turbine produces rated power (i.e. nameplate capacity). At wind speeds between the cut-in wind speed and rated wind speed, power production is calculated using Eq. 9 [68]:

$$P = \frac{1}{2} \rho A U^3 C_p \quad (9)$$

where U is the effective wind speed at the rotor, ρ is air density, A is the rotor swept area, and C_p is the power coefficient. The total power produced by the wind farm is calculated as the sum of the power produced by each turbine (Eq. 10)

$$P_{tot} = \sum_{i=1}^N P_i \quad (10)$$

In the current work, increased values of P_{tot} generally result in better objective evaluations.

3.1.1 Turbine Geometry Selection

While wind farms generally consist of a single turbine model, this work considers the possibility of many different turbine models in order to maximize power production and minimize cost by including turbine size selection capability within the turbine power production model. Wind turbine geometry selection has been successfully applied within onshore wind farm optimization, resulting in increased power production and improved objective evaluations [16,18,19,54,70]. For each turbine, the optimal turbine geometry is selected for feasible geometric relationships between rotor

radius and hub height based on commercially-available turbines. The turbine geometry selection improves the overall objective by choosing sizes that maximize power production while minimizing costs; large turbines are able to produce more power, but also have a higher cost. Large turbine sizes are chosen when the wind speed at the turbine's location provides enough power production to overcome the high cost of the turbine. The inclusion of the turbine geometry selection model allows the EPS to choose turbine geometries that optimize layout, rather than imposing an additional constraint on wind turbine size.

3.2 Wake Propagation and Interaction Model

The three dimensional wake model used in this work is derived from the PARK Model [53]. This simplified wake model is used to determine how wakes created by upstream turbines affect the wind environment at downstream turbines. Rotating blades extracting energy from the wind create a conical wake that propagates downstream. The wind speed is greatly reduced within the turbine's wake, as shown in Fig. 2. As the wake propagates, the reduced wind speed recovers asymptotically to the ambient wind speed downstream.

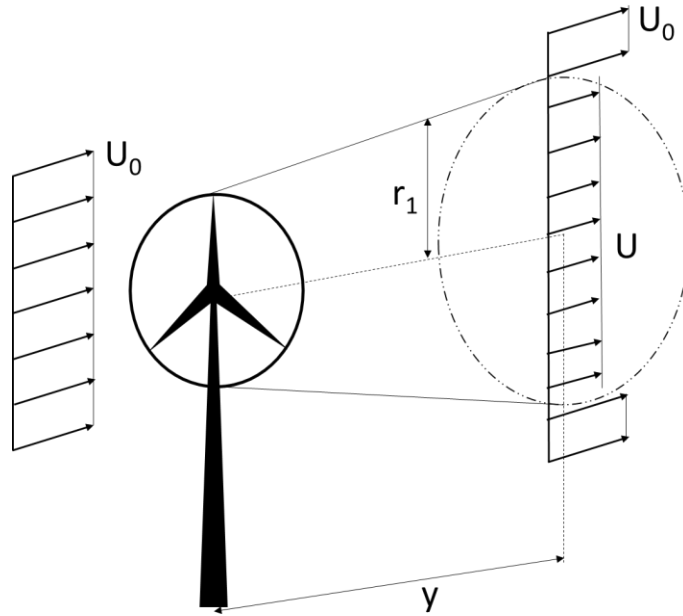


Fig. 2: Three dimensional wake propagation

The width of the wake, r_1 , and the wind speed, U , are proportional to the distance downstream from the rotor, y [16]. The free stream, or ambient, wind speed is denoted U_o . The effective wind speed at a downstream wind turbine is calculated in Equation 11. This value is the wind speed that is used in the power equation (Eq. 11):

$$U = U_o \left[1 - \frac{2}{3} \left[\frac{r_r}{r_r + \alpha y} \right]^2 \right] \quad (11)$$

where r_r is rotor radius, and α is the entrainment constant, which is calculated in Eq. 12:

$$\alpha = \frac{0.5}{\ln(z/z_0)} \quad (12)$$

where z is the hub height and z_0 is the surface roughness. The effective wind speed downstream of a rotor is plotted in Fig. 3, where the ambient wind speed is 12 m/s, the hub height is 80 m, and the rotor radius is 40 m. The wind speed is equal to one-third the ambient wind speed immediately behind the rotor.

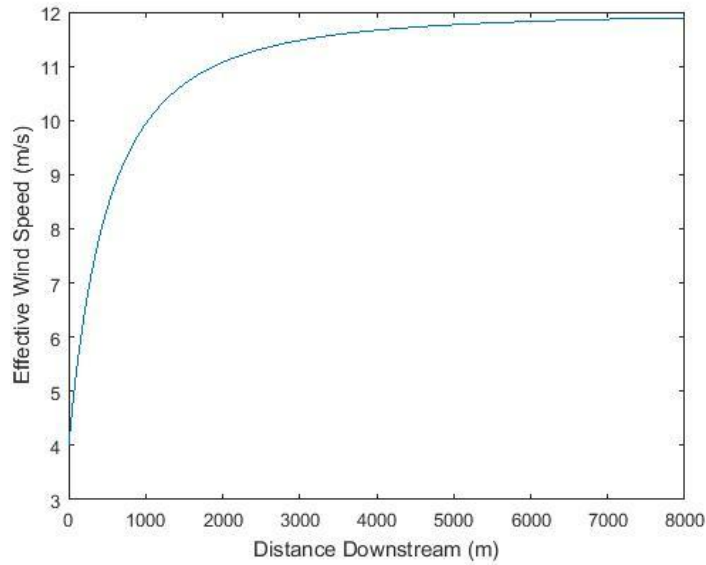


Fig. 3: Wind speed in a wake downstream of a rotor

A turbine may be affected by multiple wakes, as shown in Fig. 4.

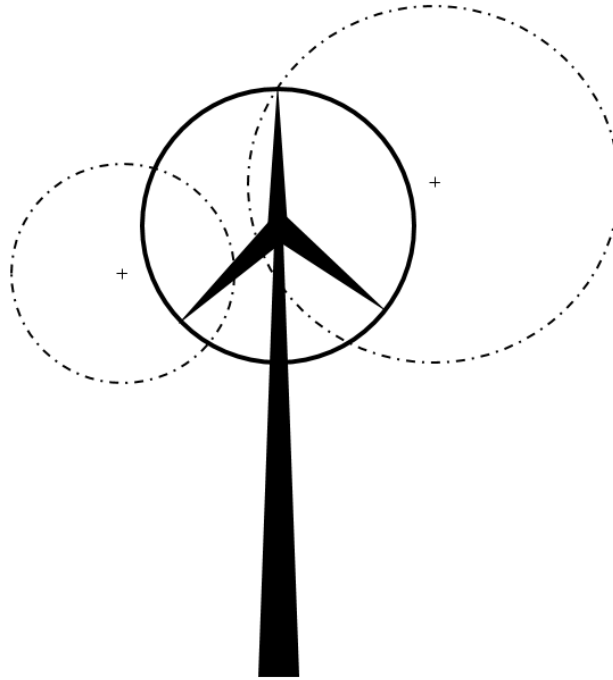


Fig. 4: Multiple wakes interacting with a rotor swept area

The equations for the effective wind speed at a downstream rotor affected by multiple wakes as well as overlapping wakes are given by DuPont et al [16,19]. For rotors in multiple, non-overlapping wakes, the wind speed is calculated as a function of the percentage of the rotor swept area in each wake. Calculating wind speed due to overlapping wakes is more complex — a 49 point discretized mesh is superimposed over the rotor swept area, and the wind speed is calculated at each discrete location. The average effective wind speed across these locations is then considered as the effective wind speed at the turbine.

3.3 Cost Model

The cost of a floating offshore wind farm is the summation of the capital, cabling, mooring, annual O&M, substation, installation, and leasing costs. Eq. 13 shows the formulation for the total cost. This cost model was developed specifically for offshore floating wind farm optimization, as a predictive model for the cost of floating turbines did not yet exist.

$$\begin{aligned}
Cost_{Total} = & Cost_{capital} + Cost_{cabling} + \\
& Cost_{mooring} + Cost_{O\&M} + Cost_{sub} + \\
& Cost_{installation} + Cost_{operating\ lease}
\end{aligned} \tag{13}$$

3.3.1 Turbine and Platform Capital Cost

The capital cost includes the costs of both the wind turbine and the WindFloat floating platform [11]. Castro-Santos references the REpower 5.075 MW wind turbine [71] that requires a semisubmersible floating platform of mass 695,985 kg [72]. The cost of this wind turbine is \$1.32 million/MW. The cost of the semisubmersible platform is \$575.65/ton, or \$400,644 for a platform supporting a 5.075 MW turbine. The total cost of the 5.075 MW turbine and semisubmersible platform is \$1.48 million/MW, as shown in Eq. 14:

$$Cost_{capital} = P_{rated,farm} \times \$1.48 \text{ million} \tag{14}$$

where $P_{rated,farm}$ is the rated power of the entire farm in MW, given in Eq. 15:

$$P_{rated,farm} = \sum_{i=1}^N P_{rated,turbine,i} \tag{15}$$

where N is the number of turbines in the farm and $P_{rated,turbine}$ is the rated power of each turbine.

3.3.2 Cabling Cost

The cabling system for a floating offshore wind farm is comprised of two types of cables: inter-array cables and export cables. Inter-array cables connect turbines in the array to a single location, such as a turbine at the front of the farm. The power is sent to an onshore substation via an export cable.

The cost of inter-array cabling is \$307,000/km. Equation 16 calculates the cost for the inter-array cabling of the entire farm [73]:

$$C_{inter-array} = d_t \times \$307,000 \quad (16)$$

where d_t is the total length of the inter-array cables. The cost of the export cables relies on the distance between the substation and shore, d_s , in kilometers. The cost of export cabling is \$492,000/km. Equation 17 gives the cost for the export cabling [73].

$$Cost_{export} = d_s \times \$484,000 \quad (17)$$

Equation 18 determines the total cost of cabling, which is the sum of the inter-array and export cabling costs.

$$Cost_{cabling} = Cost_{inter-array} + Cost_{export} \quad (18)$$

3.3.3 Anchoring and Mooring Cost

The equations for the cost of anchoring and mooring are derived from work by both Castro-Santos et al. [46,74] and Myhr et al. [73]. Castro-Santos et al. considers 21 5.075-MW turbines on semisubmersible floating platforms off the Galician Coast in Northern Spain [74]. The WindFloat is anchored to the seafloor using drag embedment anchors [75]. The total manufacturing cost for each anchor is \$9,943, or \$39,772 for four anchors. Myhr et al. consider a WindFloat moored in 200 meter water depth (h), requiring 200 meters of chain mooring and 2640 meters of steel wire [73]. The chain costs \$274/meter and the steel wire costs \$49.32/meter. As water depth changes, the length of a single chain is equal to the water depth, which will cost \$274/meter of water depth, or \$1096/meter of water depth for 4 lines. The length of the steel wire is constant at 2640 meters, which cost \$520,820 for four lines. Equation 19 calculates the total anchoring and mooring cost for the wind farm, assuming four lines are attached to the WindFloat platform [75].

$$C_{mooring} = N \times (\$39,772 + \$520,820 + \$1,096 \times h) \quad (19)$$

3.3.4 Annual Operations and Maintenance Cost

This work uses the O&M cost suggested by the NREL Jobs and Economic Development (JEDI) Model for Offshore Wind Farms [76]. The JEDI Model uses an annual cost for O&M of \$133/kW for an offshore wind farm. Total O&M cost in the JEDI model is a function of the size of the wind farm ($P_{Rated,Farm}$) and the length of the project in years (t), given in Equation 20, where $P_{Rated,Farm}$ is in megawatts.

$$C_{O\&M} = \$133,000 \times P_{Rated,Farm} \times t \quad (20)$$

3.3.5 Substation Cost

Two options are available for substation cost: (1) a floating offshore substation and (2) a traditional onshore substation. The offshore substation cost includes both the manufacturing cost and installation cost of a floating offshore substation. According to Myhr et al., the capital cost for a 500 MW offshore substation is \$177.24 million, and the installation cost is \$20.39 million [73]. For a 1000 MW substation, the capital cost is \$297.81 million and the installation cost is \$31.24 million. Equation 21 calculates the total capital and installation cost for a floating offshore substation as a function of the rated power of each wind turbine:

$$Cost_{sub} = (\$262840 \times P_{rated,farm}) + \$66,210,000 \quad (21)$$

where $P_{rated,farm}$ is in megawatts.

Onshore substation costs are based on real projects for substations built for wind farms and solar farms [77]. The baseline cost of a substation is \$2 million, with costs increasing linearly as the size of the farm grows, as shown in Eq. 22.

$$Cost_{sub} = \$20,000 \times P_{rated,farm} + \$2,000,000 \quad (22)$$

According to the research used to develop the substation cost model, offshore substations are less economically feasible than onshore substations. As such, it is assumed that onshore substations will be used for the wind farms developed through this work; the cost of these substations is given in Eq. 22.

3.3.6 Installation Cost

Castro-Santos identifies installation costs for the wind turbine, platform, mooring and anchoring, electrical, and commissioning (Eq. 23) [72].

$$C_{installation} = \$977,620 \times N \quad (23)$$

3.3.7 Leasing Cost

The Bureau of Offshore Energy Management (BOEM) is in charge of regulating and leasing Outer Continental Shelf (OCS) area. Their role is to coordinate with all involved federal agencies, states, and local governments in order to ensure development is safe and environmentally-responsible, as well as obtain fair return for issued leases and grants [78]. A lessee begins paying “operating fees” once commercial generation of electricity has begun. Equation 24 can be used to calculate the cost of the operating lease [79]:

$$C_{operating\ lease} = P_{rated,farm} \times 8760 \times c_f \times COE \times r \times t \quad (24)$$

where 8760 is the total number of hours in a year, c_f is the capacity factor (0.4); COE is the annual average wholesale electric power price, r is the operating fee rate (equal to 0.02 for the first 8 years of operation, and 0.04 for the rest of the lease), and t is the length of the lease in years [79].

3.3.8 Other Cost Considerations

The decommissioning cost is assumed to be negligible and will not be included in this model [72]. This work does not optimize the layout of mooring or inter-array cabling. The farm layouts determined from this work will inform optimal mooring and cabling configurations in future research, to further drive down costs.

3.3.9 Onshore Cost Model

The optimized offshore layouts are compared to onshore layouts with similar parameters. The cost model for the onshore wind farm model is based on the polynomial cost surface as a function of rotor radius and hub height by DuPont et al. [16].

Chapter 4: Extended Pattern Search Approach

4.1 Introduction

EPS methods are ideal for optimizing multi-variable, multi-modal problems by combining a deterministic pattern search algorithm with stochastic extensions. The first two extensions ensure that the EPS traverses in a randomized manner, preventing favoring the selection or movement of any agent. The third extension helps the algorithm avoid stopping at poorly performing local optima. The EPS framework allows for the inclusion of advanced models, such as those used in this work for cost, power production, turbine geometry selection, and wake propagation/interaction. New models can be easily incorporated as technologies for offshore wind farms continue to advance.

The pseudocode shown in Fig. 5 shows how the three extensions are integrated into the pattern search, and can be used to understand the functionality of the EPS described in this work.

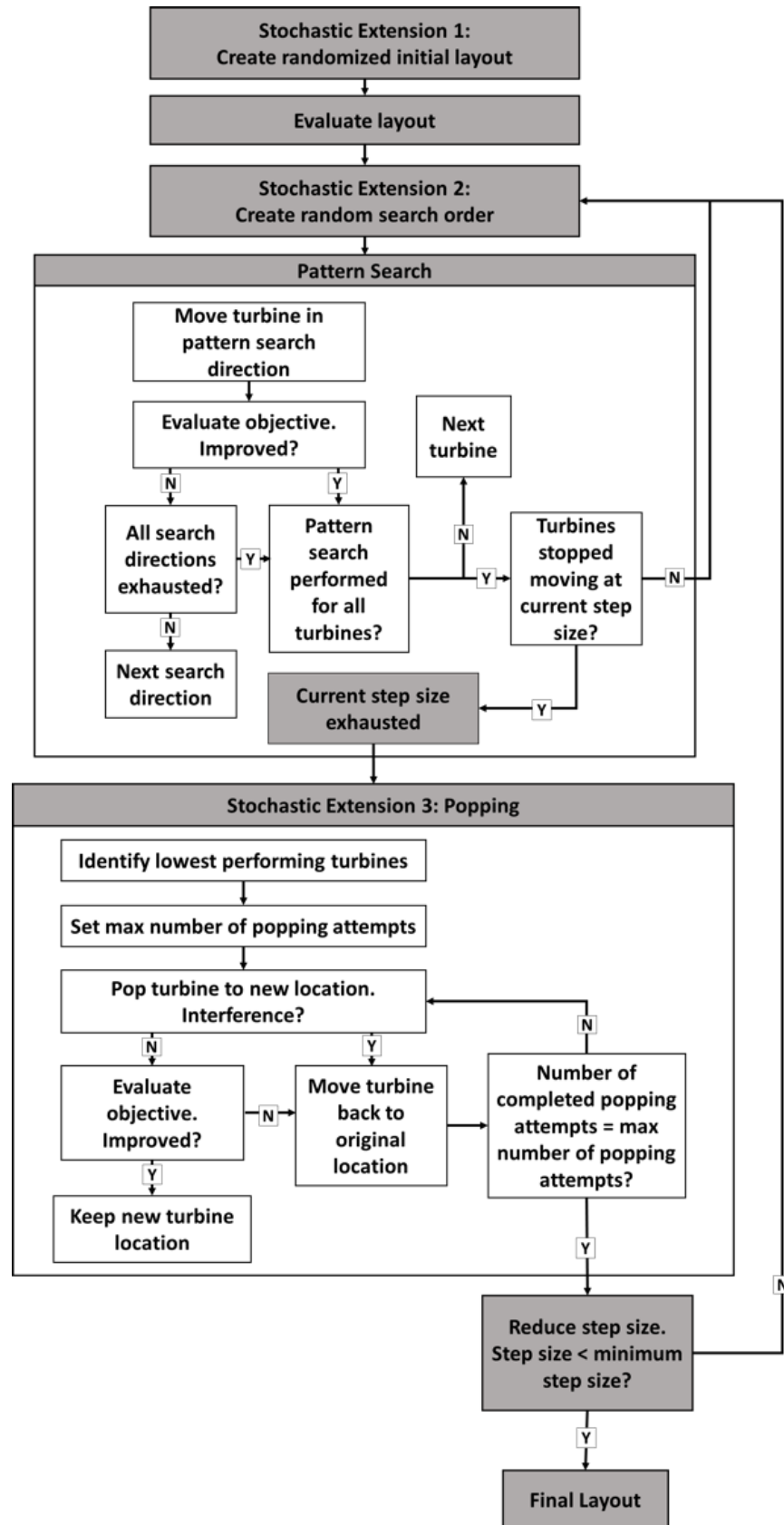


Fig. 5: EPS Pseudocode

4.2 Pattern Search

Pattern search algorithms, such as the one incorporated in the EPS used in this work, are a type of direct search algorithm as introduced by Hooke and Jeeves that do not require the calculation of derivatives [80,81]. Pattern search algorithms are deterministic, robust, and computationally inexpensive, but do not perform well alone in multi-modal optimization.

As depicted in the “Pattern Search” box in Fig. 1, the pattern search begins by evaluating the objective function. Then, an agent (in this case, an offshore floating wind turbine) is moved in the first pattern search direction at an initial step size. The objective function is then evaluated again; the move is kept if it has improved the overall objective evaluation. If not, a step at the initial step size is taken in the next pattern search direction. Once an agent is no longer able to accept steps, the pattern search moves onto the next agent in the layout. This process is continued until all agents are no longer moving at the initial step size. Once agents are no longer accepting moves, the step size is reduced and the pattern search begins again. The pattern search is stopped once the step size has been reduced below a user-defined lower bound step size.

4.3 Stochastic Extensions

Combining stochastic extensions with the deterministic pattern search increases the ability of the algorithm to find better-performing layouts in multi-modal spaces. Yin and Cagan introduced stochastic extensions for three-dimensional component layout optimization that demonstrated increased convergence over a robust simulated annealing algorithm [82]. Three stochastic extensions are included in this work: (1) randomized initial layout, (2) randomized search order, and (3) a popping algorithm. Each extension increases the stochasticity of the EPS.

4.3.1 Randomized Initial Layout

The first stochastic extension occurs only once, at the beginning of the algorithm. An initial layout is created with turbines positioned at randomly-generated locations in

the search space. Turbines must be placed at least five rotor radii away from other turbines; otherwise, turbines can be placed anywhere within the search space.

4.3.2 Randomized Search Order

The second stochastic extension occurs at the beginning of each pattern search. The order that the pattern search follows for each turbine is randomly generated for each new step size. This extension reduces the chances of biasing turbines, since changing the position of individual turbines can affect the power production of surrounding turbines due to changes in wake effects.

4.3.3 Popping

The third stochastic extension occurs when the pattern search at each step size has been exhausted. The popping algorithm takes a user-defined number of poorest-performing agents and “pops” them to new, random locations in the search space. The new, popped locations are evaluated to determine if they improve the overall objective evaluation, and are checked for proximity to other turbines. If the new location improves the objective and is at least five rotor radii from other turbines, the new location is kept. Otherwise, the turbine is moved back to its original location, and popped to new locations until it has found a better location, or a maximum number of popping attempts has been reached.

4.4 Objective Function

This work uses a profit objective function to determine the success of layouts (Eq. 25). The objective function can be used by developers to determine the expected cost and power production of offshore floating wind farms containing a certain number of turbines at a given configuration.

$$Objective = Cost_{total} - (P_{tot} \times c_f \times COE \times t) \quad (25)$$

where $Cost_{total}$ is the total cost of the wind farm (Eq. 13), P_{tot} is the total power produced by the farm (Eq. 10), c_f is the capacity factor, COE is the cost of electricity, and t is the total number of operational hours. Equation 25 is given in negative null form; the objective function is optimized by simultaneously minimizing the total cost and maximizing the total power production.

4.5 Stopping Criteria

Due to the multi-modality and both discrete and continuous nature of the wind farm layout optimization problem and EPS, global convergence is not guaranteed. Instead, stopping criteria are defined to determine when the EPS has sufficiently exhausted potential layouts. The popping algorithm has two stopping criteria: either all low-performing turbines have been moved to new locations, or a user-defined maximum number of popping iterations has been reached. The stopping criterion for the EPS occurs after a user-defined minimum step-size pattern search has been exhausted.

Chapter 5: Problem Formulation

5.1 Unidirectional Wind Case

The first wind case explored in this work is unidirectional, single wind speed as shown in Fig. 6. The free stream wind speed is constant, approaching from the bottom of the field. For the comparison of the onshore and offshore layouts, the wind speed is 10 m/s; for the comparison of the EPS and Adapted GA, the wind speed is 12 m/s. The layouts are optimized within a 4000 m by 4000 m flat space. Water depth is 200 m and the farm is 30 kilometers from shore. The life of the farm is 20 years.

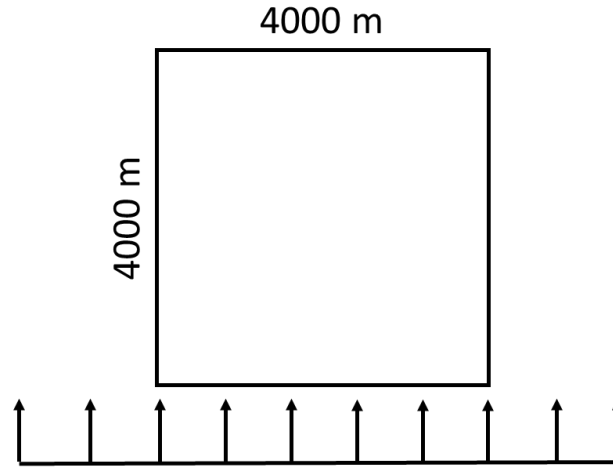


Fig. 6: Unidirectional wind case

The offshore layouts are compared to onshore layouts of the same size and wind speed. Surface roughness for onshore wind farms over a fallow field has an experimental value of $z_0 = 0.03$ meters, whereas the surface roughness of a calm open sea has an experimental value of $z_0 = 0.0002$ meters [68]. The wind profile power law is (Eq. 26):

$$\frac{u}{u_r} = \left(\frac{z}{z_r}\right)^{\alpha_h} \quad (26)$$

where u_r and z_r are reference wind speed and heights, respectively. The power law exponent is $\alpha_h = 0.11$ for most offshore locations and stability conditions [5,83]. The onshore power law exponent is $\alpha_h = 0.1$ (unstable), $\alpha_h = 0.15567$ (neutral), and $\alpha_h = 0.2$ (stable) [16].

The number of popping attempts is set to 1000 for the poorest performing 10 turbines at each step size. Table 1 includes the parameters for the onshore and offshore wind layouts.

Table 1: Offshore and onshore wind farm parameters

	Offshore	Onshore
Wind Speed	10 m/s	10 m/s
Farm Length	4000 m	4000 m
Water Depth	200 m	----
Life of Farm	20 years	20 years
Distance from Shore	30 km	----
Surface Roughness	0.0002 m	0.03 m
Power law exponent	0.11	0.1 (unstable)/ 0.15567 (neutral)/ 0.2 (stable)
Number of popping attempts	1000	1000
Number of popped turbines	10	10

The EPS for the offshore case is compared to an Adapted Genetic Algorithm [29]. The wind case used is that of unidirectional wind and a single wind speed of 12 m/s approaching from the bottom of the field (Fig. 6). Since the wind speed and direction are constant, efficiency is simplified and can be determined using Eq. 27:

$$\eta = \frac{P_{tot}}{N \times P(u)} \quad (27)$$

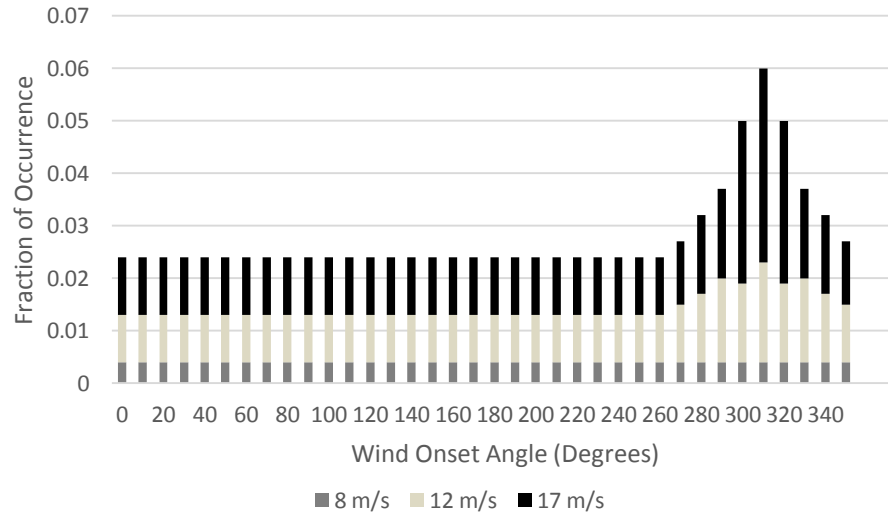
where P_{tot} is the total power produced by the farm, and $P(u)$ is the power produced by each turbine when the wind speed at the rotor is equal to the ambient wind speed, 12 m/s. The farm area is a square with side lengths equal to 4000 m. The rated wind speed for each turbine is 14 m/s and rated power is fixed at 5 MW. Rotor radius is calculated to be 43.5 m, and hub height is not given, but is assumed to be 90 m (Table 2).

Table 2: EPS and Adapted GA comparison parameters

Ambient wind speed	Rated wind speed	Rated power	Grid size	Hub Height
12 m/s	14 m/s	5 MW	4 km x 4 km	90 m

5.2 Multidirectional Wind Case

In this work, wind farms are optimized in a square space with side lengths equaling five kilometers. A multidirectional, multiple wind speed wind case is used (Fig. 7). The zero-degree onset angle is entering the bottom of the field, moving clockwise around the field with increasing angles.

**Fig. 7:** Wind onset angle and fraction of occurrence for multidirectional, multiple speed wind case

Surface roughness of a calm open sea has an empirical value of $z_0 = 0.0002$ meters [68]. The power law exponent, α_h , is equal to 0.11 for most offshore locations and stability conditions [5,83]. The worst-performing 10 turbines are popped in the third stochastic extension; the maximum number of popping attempts is 100. The wind farm is expected to have a 20-year lifetime. The water depth is 200 meters, and the distance from shore is 30 kilometers. The offshore wind farm parameters are given in Table 3.

Table 3: Offshore environment characteristics

Side length	2000 m
Water Depth	200 m
Life of farm	20 years
Distance from shore	30 km
Surface Roughness	0.0002 m
Power law exponent	0.11
Number of popping attempts	100
Number of popped turbines	10

The study presented in this work explores layouts and turbine geometries optimized for wind farms containing one to 22 turbines. Suggested layouts are presented for wind farms subjected to the wind climate presented in Fig. 6.

5.3 Hard-Coded Layout Study

Wind farm layouts are evaluated for two wind cases. Case 1 is a unidirectional wind case with constant wind speed at 10 m/s entering from the bottom of the field, in the +y direction (Fig. 6). Case 2 is a multidirectional wind case using wind speeds of 8 m/s, 12 m/s, and 17 m/s and 36 wind directions with varying probabilities of occurrence for each wind direction (Fig. 7) [19]. The Siemens SWT 3.6-107 turbine is used for this study [84]; its hub height is 80 meters and rotor radius is 53.5 meters. The life of each wind farm is 20 years. Each solution space is a square with side lengths of 2000 meters. Offshore atmospheric conditions are used in the model; the surface roughness z_0 is 0.0002 meters [68] and the power law exponent α_h is 0.11 [5,83].

Nine layouts were developed based on the common patterns from offshore wind farm layout optimization literature (Fig. 8). All nine layouts are tested for both Case 1 and Case 2.

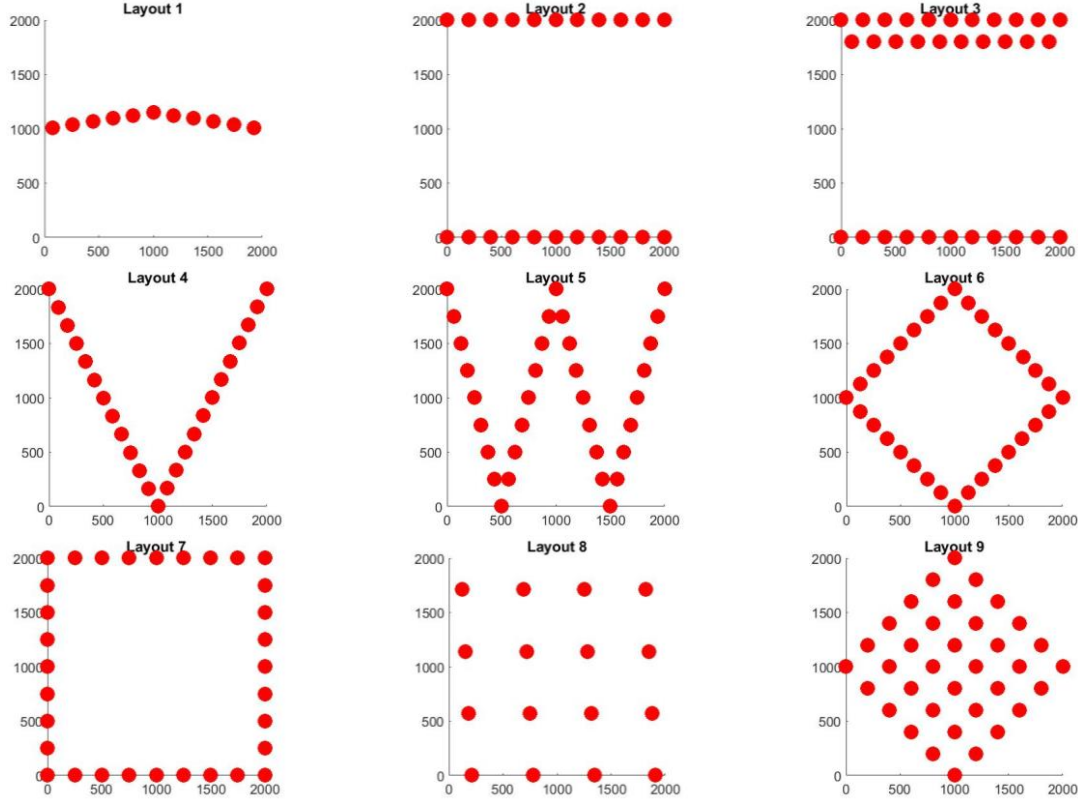


Fig. 8: Empirically-derived wind farm layouts

5.4 Seeded Initial Layout Study

The purpose of this study is to reduce the noisiness of the data in the Unidirectional Wind Case study (5.1) by seeding initial layouts with layouts known to be good based on the results from the Hard-Coded Layout Study (5.3). The studies described in Sections 5.1 and 5.2 use an EPS with all three stochastic extensions as described in Section 4.3, including the randomized initial layout. In this study, however, the use of informed initial layouts is explored. The use of targeted initial populations has been studied within genetic product searches [85,86]. While the use of randomly generated initial populations in genetic algorithms increases the genetic diversity in solutions, using domain knowledge to create targeted initial populations can significantly improve results in large-scale problems [85,86]. Foster and Ferguson used customer preference information to create target initial populations for both single and multi-objective Genetic Algorithms in the design of product lines, resulting in better solutions and faster convergence [85]. For a single objective GA in the design of MP3 players,

the use of targeted initial populations always performed better than solutions found using random initial populations [85]. Foster et al. gathered preference information data from customer surveys to inform targeted initial populations, and found that products that perform well for a portion of the market perform better for the entire market than products that are generated randomly [86]. In addition, using targeted populations reduced the computational cost of genetic product searches [86]. Maaranen et al. also studied the effects of various initial population generation techniques on the success of GAs on simple problems [87]. While the numerical results were not strong enough to make firm conclusions, it was found that GAs with good genetic diversity in their initial populations converged quickly, but, on average, did not obtain the best final objective values [87].

In this study, initial populations are used based on the results from the Hard-Coded Layout Study (5.3). Results indicate that farms containing rows of wind turbines perpendicular to the wind direction perform best in unidirectional wind cases (Fig. 8). Two cases are presented: (1) a 4000 m by 4000 m space, and (2) a 2000 m by 2000 m space. In Case 1, farms containing between 16 and 52 wind turbines are optimized. The wind turbines are placed along four rows, as seen in Fig. 9.

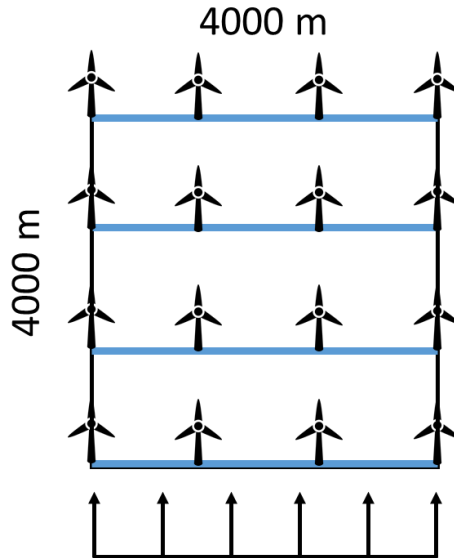


Fig. 9: Initial layout for a wind farm with side lengths of 4000 m

In Case 2, farms containing between four and 48 wind turbines are optimized. The wind turbines are placed along 7 rows, as shown in Fig. 10.

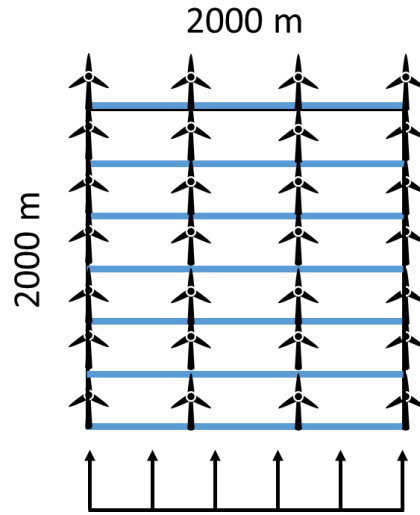


Fig. 10: Initial layout for a wind farm with side lengths of 2000 m

Resulting objective evaluations from the farms optimized using seeded initial layouts are compared to farms optimized using random initial layouts. Unless otherwise noted, all other parameters for this study are given in Section 5.1.

Chapter 6: Unidirectional Wind Case Results and Discussion

6.1 Results

Layouts were optimized for farms containing between 15 and 60 turbines for both onshore and offshore environments using the parameters given in Table 1. Each set of results was generated five times. The least-error relationship between number of turbines and the objective function is determined to be quadratic for the offshore environment (Fig. 11, $R^2 = 0.5597$) and cubic for the onshore environment (Fig. 12, $R^2 = 0.3909$). The hub height and rotor radius of each turbine are indicated the key given in Fig. 13. The offshore environment has a minimum objective evaluation when the layout is optimized for 42 turbines; the minimum objective evaluation for a 42 turbine layout is -1.79456×10^8 (Fig. 14). The cost of cabling for the 42 turbine layout is approximately $\$1.9432 \times 10^7$, resulting in an objective function evaluation equal to -1.60024×10^8 (Table 4). The onshore environment has a minimum objective evaluation when the layout is optimized for 32 turbines; the minimum objective evaluation for a 32 turbine layout is -1.64933×10^8 (Fig. 15).

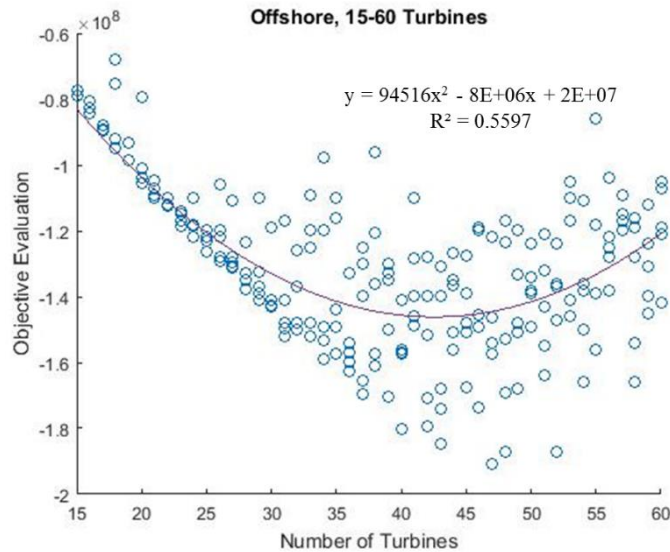


Fig. 11: Objective evaluation for offshore layouts containing 15 to 60 turbines

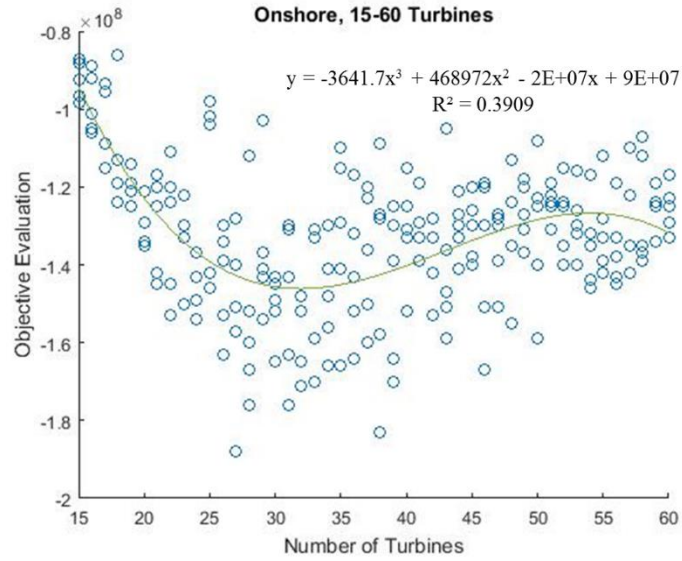


Fig. 12: Objective evaluation for onshore layouts containing 15 to 60 turbines

Hub Height (m)		Rotor Radius (m)	
○	≤ 60	Red	≤ 30
△	60-80	Yellow	30-40
◇	80-120	Green	40-60
□	>120	Blue	>60

Fig. 13: Turbine geometry key

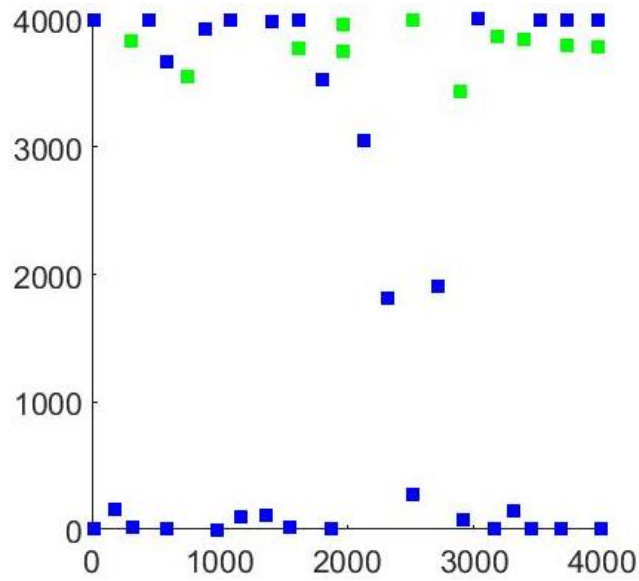


Fig. 14: 42-turbine offshore layout, objective evaluation = $-1.79456e+08$

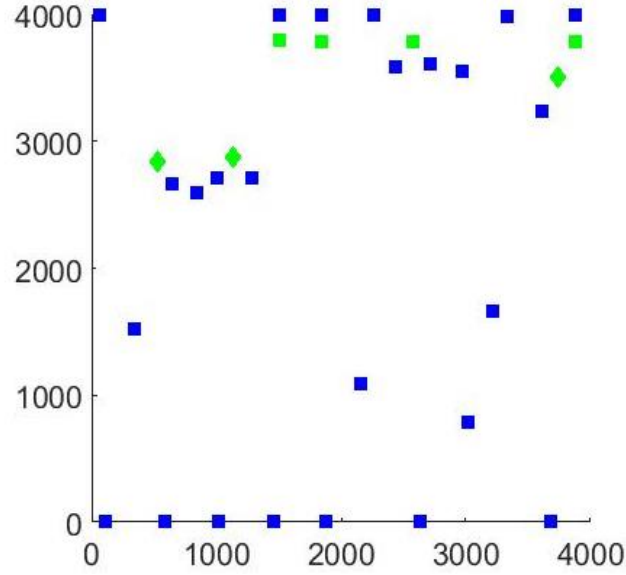


Fig. 15: 32-turbine onshore layout, objective evaluation = $-1.64933\text{e}+08$

Table 4: Minimum objective evaluations for offshore and onshore layouts

	Offshore	Onshore
Optimal Number of Turbines	42	32
Minimum Objective Evaluation	$-1.79456\text{e}+08$ ($-1.60024\text{e}+08$)	$-1.64933\text{e}+08$
R^2 Value	0.5597	0.3909

Layouts were optimized for an offshore environment based on parameters given in Table 2. A 16-turbine layout was generated using the EPS and compared to the layout generated using the Adapted GA [29] (Figs. 16 and 17). Efficiencies (Eq. 27) for layouts containing between 15 and 60 turbines are shown in Fig. 18. Layouts generated by the EPS are 100% efficient up to 34 turbines (Fig. 19).

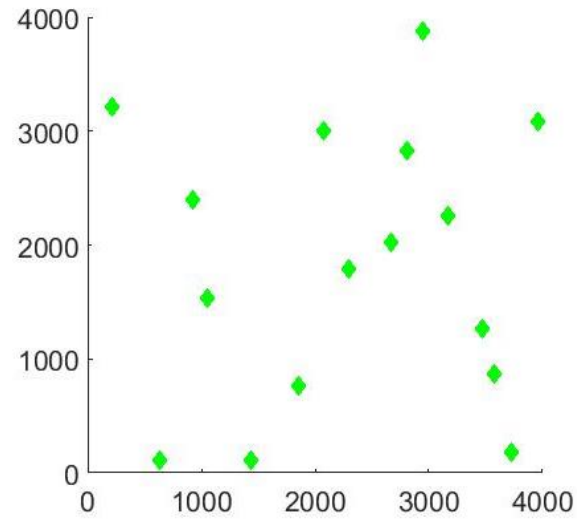


Fig. 16: 16-turbine layout, EPS, 100% efficiency

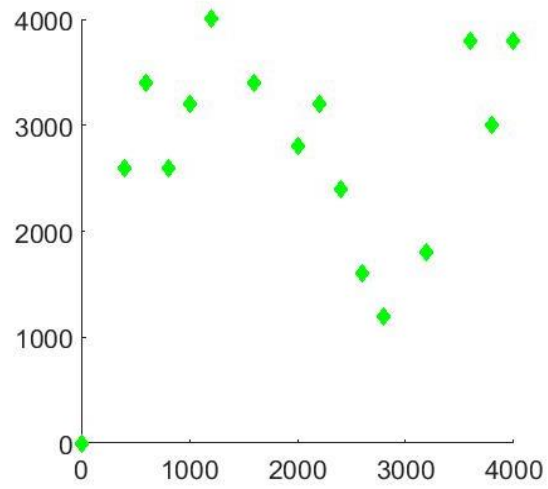


Fig. 17: 16-turbine layout, Adapted GA, 100% efficiency (Liu and Wang [29])

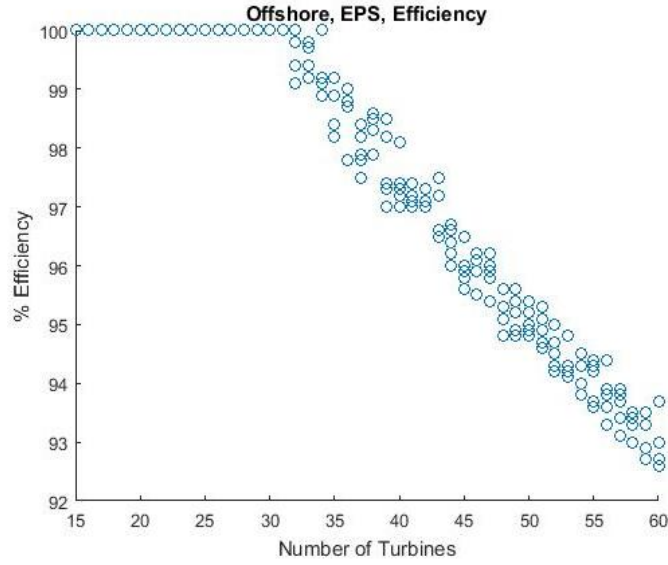


Fig. 18: Efficiency of EPS-generated layouts

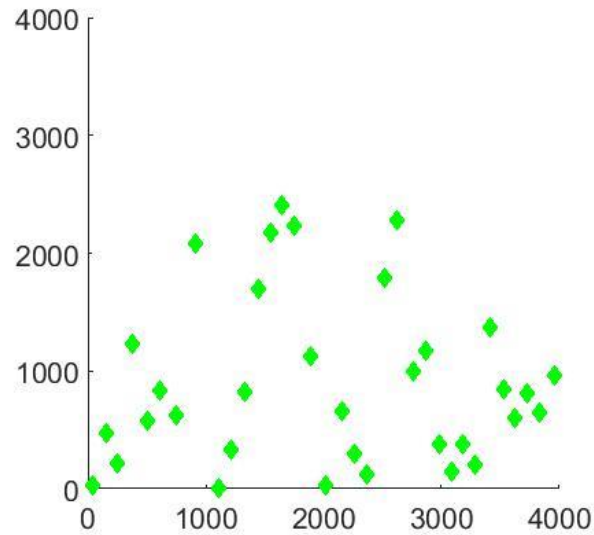


Fig. 19: 34-turbine layout, EPS, 100% efficiency

6.2 Discussion

The deviation in the optimal number of turbines between the onshore and offshore minimum objective evaluations can be attributed to three differences: cost, surface roughness, and power law exponent. The surface roughness and power law exponents for both onshore and offshore environments are given in Table 1. These values affect the wind speed with respect to elevation and the shape of a wake behind a rotor. Changing these values affects where the EPS places turbines in reference to other

turbines, since the turbine agents try to avoid being placed in wakes. However, the change in cost more greatly affects the optimal number of turbines as evaluated by the objective function. Higher investment in offshore wind farms are required for them to be as profitable as onshore wind farms due to higher initial costs. However, results from this work indicate that offshore wind farms may be as profitable as onshore wind farms over a 20-year lifetime. It should be noted that the cost model used in this work is new, and it has inherent uncertainty that propagates throughout the execution of the optimization algorithm. That, coupled with the relative simplicity of the indicated wind cases (unidirectional, single-wind-speed) limit the real-world applicability of the current method. Objective evaluations determined in this work may not represent actual profit margins for real wind farms; however, subsequent improvement to the utilized modeling will be conducted to improve accuracy.

The layouts shown in Figs. 14 and 15 contain large turbines populating the front and back of the field, with turbines scattered throughout the middle of the field. The turbines at the front of the field are unaffected by wakes, and are able to extract the most energy from the ambient wind speed. The turbines at the far back of the field have spread out in order to move far away from the wakes of upstream turbines; this is commonly seen in optimized wind farm layouts [16–19]. For the offshore layout, most turbines are within the largest rotor radius and hub height group, indicating that the power they are able to generate outweighs the increase in cost caused by the increased size of the turbines. The layouts shown in Figs. 14 and 15 are selected based on their objective evaluations; it is important to note that the common behavior across layouts are shown in these figures, but it may be possible to improve the location of individual turbines.

The noise in the data for both the onshore and offshore objective evaluations is due to the randomness of the EPS (Figs. 11 and 12). The three stochastic extensions help to avoid settling on poor-performing local optima. However, factors such as poor initial layouts or insufficient popping attempts can lead to variation in the objective evaluation for layouts containing the same number of turbines. Additionally, the application of a continuous algorithm to a large solution space allows infinitely many possible turbine

locations and, given a lack of guaranteed global convergence of the EPS, the algorithm is likely to settle on local optima.

The efficiency of the 16 turbine layouts for both the Adapted GA and EPS are 100%. However, this may be attributable to the large area of the farm; turbines are able to easily spread out at this size to reach optimal efficiency. As the number of turbines in the farm increases, the more difficult it becomes for the farm to be theoretically perfectly efficient. Layouts with more than 16 turbines are not provided for the Adapted GA, therefore, the greatest number of turbines in a farm at 100% efficiency cannot be compared to the EPS [29]. However, the Adapted GA requires the field area to be discretized into 200 m by 200 m sections, limiting the number of possible layout solutions. The EPS is able to optimize continuously within the field area such that a greater number of highly efficient layouts are possible.

Chapter 7: Multidirectional Wind Case Results and Discussion

7.1 Results

Layouts were optimized using the EPS for farms containing between one and 22 turbines. The objective evaluation for each layouts is plotted against the number of turbines in the layout in Fig. 20. Based on a cubic fit to the data (with an R^2 value of 0.9026), the projected minimum objective evaluation occurs when the wind farm contains five turbines. The objective evaluation for the best layout containing five turbines is $-\$9.93 \times 10^6$ (Fig. 22); the hub height and rotor radius of turbines can be interpreted using the turbine geometry key given in Fig. 21. The average power production for the five turbine layout is equal to 23.4 MW. The overall minimum objective evaluation for the data shown is equal to $-\$1.20 \times 10^7$ for a seven turbine layout (Fig. 23). The average power production for the seven turbine layout is equal to 28.7 MW.

A 12-turbine layout was generated that also has a low objective evaluation ($-\$8.96 \times 10^6$, Fig. 24). The average power production of the 12-turbine layout is 42.2 MW.

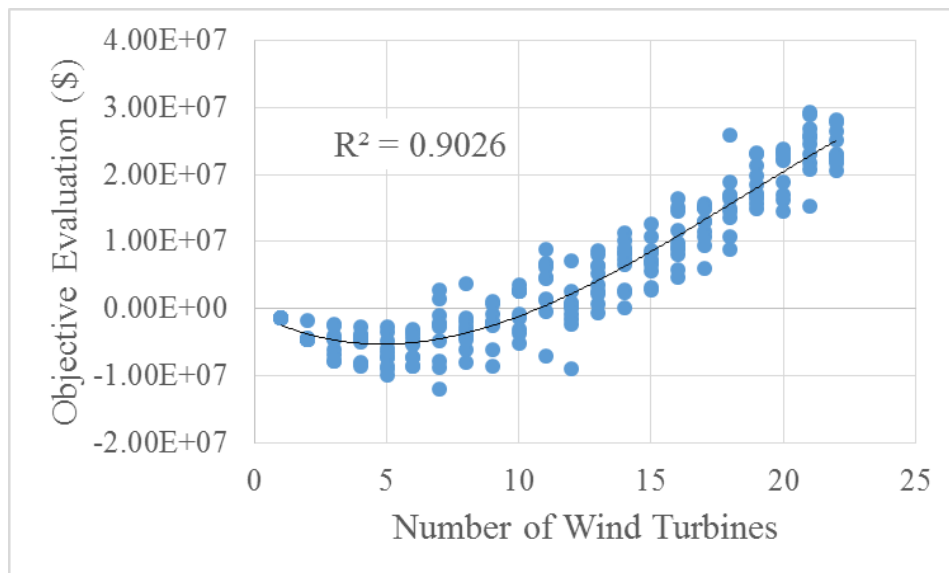


Fig. 20: Objective Evaluation for layouts containing one to 22 turbines




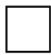
Hub Height (m)		Rotor Radius (m)	
	≤ 60	Red	≤ 30
	60-80	Yellow	30-40
	80-120	Green	40-60
	>120	Blue	>60

Fig. 21: Turbine geometry key

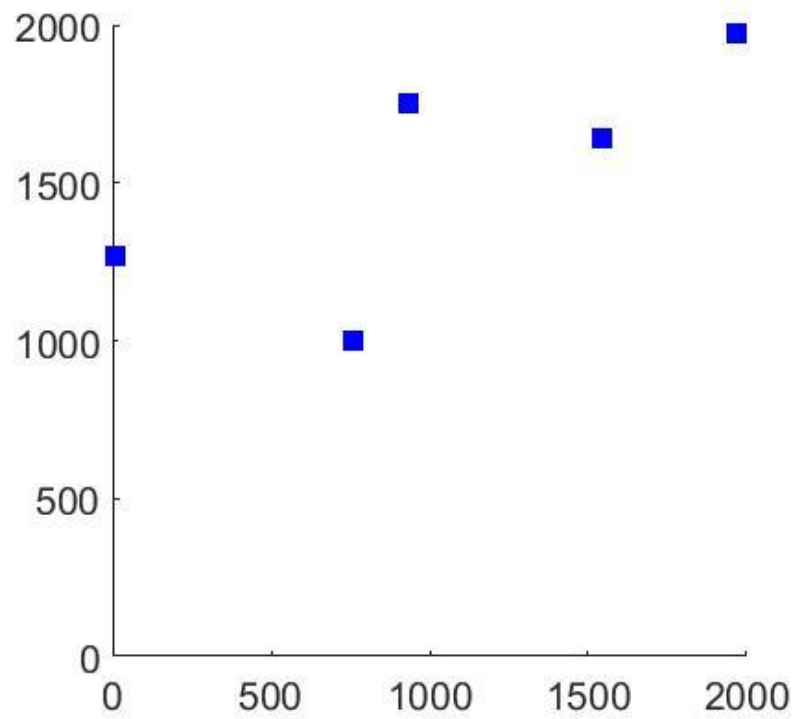


Fig. 22: Optimized layout containing five turbines, objective evaluation = $\$9.93 \times 10^6$

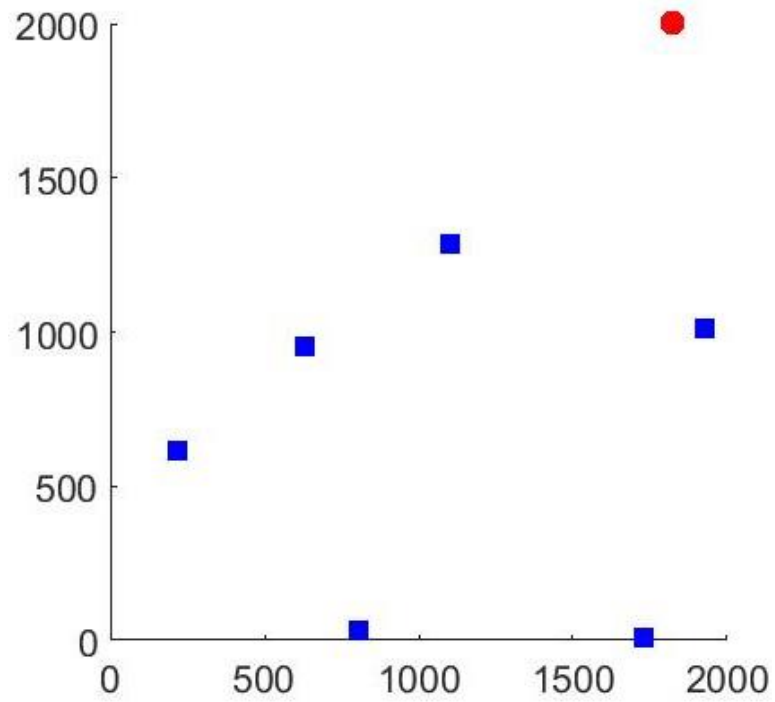


Fig. 23: Optimized layout containing seven turbines, objective evaluation = -
 $\$1.20 \times 10^7$

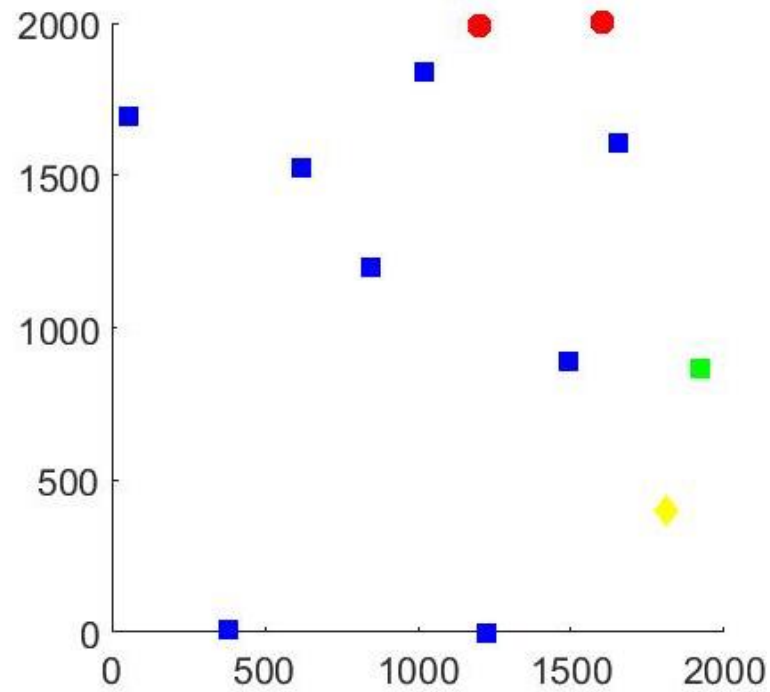


Fig. 24: Optimized layout containing 12 turbines, objective evaluation = - $\$8.96 \times 10^6$

7.2 Discussion

The layouts given in Figs. 22 and 23 have similar characteristics; they line up in perpendicular rows, diagonally across the field, from the bottom left corner to the top right. In the $40^\circ - 60^\circ$, and $220^\circ - 240^\circ$ onset angle wind directions, wake losses are more significant than in other directions. The turbines are lined up perpendicularly to the $310^\circ - 320^\circ$ wind directions, which experience higher wind speeds (Fig. 7). This means that along the $310^\circ - 320^\circ$ wind directions where the highest wind energy occurs, wake interactions are minimized; this behavior is expected of optimal layouts. The five turbine layout shown in Fig. 22 implemented wind turbines of the largest rotor radii and hub heights. This suggests that the power production of each turbine was high enough to overcome the high costs of implementing large turbines. However, the seven turbine layout shown in Fig. 23 implemented one turbine of the smallest available turbine geometry. It is likely that the EPS did not find a location for this turbine that would allow it to produce enough energy to overcome the high costs, and instead made it as small as possible, both to reduce costs and to help it avoid the wakes of upstream turbines.

The 12-turbine layout shown in Fig. 24 is included to show the behavior of a wind farm containing a higher number of turbines. The 12-turbine layout has some similar behavior as the five and seven-turbine layouts. However, turbines that are not aligned diagonally are placed along the perimeter of the field. This behavior is common among multidirectional wind farm optimization [16,54]. The 12-turbine layout implements four unique turbine geometries ranging in both rotor radius and hub height. By allowing the EPS to choose the turbine geometry, it is able to further minimize the objective function; if only a single wind turbine hub height and rotor radius were allowed, the resulting layout would have been less optimal than the one shown in Fig. 24.

Chapter 8: Hard-Coded Layout Study Results and Discussion

8.1 Results

Layouts were hard-coded in the model and evaluated for both Case 1 and Case 2 (Table 5). Minimized transmission cable layouts were determined for each layout (Fig. 8). Results for the objective evaluation both including and excluding the cost of cabling are given. In addition, the average Annual Energy Production (AEP) per turbine for each layout are given.

For Case 1, Layouts 1 and 2 have the lowest objective evaluations and highest AEP per turbine. For Case 2, Layouts 2 and 8 have the lowest objective evaluations and highest AEP per turbine.

Table 5: Objective Evaluation and AEP Results for Layouts 1-9, Cases 1 and 2

Layout	Number of Turbines	Case 1 (Unidirectional)			Case 2 (Multidirectional, 3 Speeds)		
		Objective Evaluation (\$)	Objective with Cabling (\$)	AEP/ turbine (Watts)	Objective Evaluation (\$)	Objective with Cabling (\$)	AEP/ turbine (Watts)
1	11	-1.73E+07	-1.68E+07	9.65E+09	-4.17E+07	-4.11E+07	1.20E+10
2	22	2.65E+07	2.83E+07	8.21E+09	-9.71E+07	-9.52E+07	1.23E+10
3	32	1.03E+08	1.05E+08	7.19E+09	1.92E+07	2.15E+07	9.47E+09
4	25	8.53E+07	8.67E+07	7.10E+09	-5.07E+06	-3.70E+06	9.93E+09
5	33	3.28E+08	3.31E+08	3.83E+09	8.37E+07	8.62E+07	8.39E+09
6	32	1.19E+08	1.20E+08	6.95E+09	7.79E+07	7.96E+07	8.45E+09
7	32	2.89E+08	2.92E+08	4.28E+09	-7.06E+07	-6.81E+07	1.10E+10
8	16	1.74E+08	1.77E+08	3.38E+09	-8.40E+07	-8.14E+07	1.28E+10
9	36	3.80E+08	3.83E+08	3.52E+09	1.64E+08	1.67E+08	7.26E+09

8.2 Discussion

The two best-performing layouts for Case 1 have rows of turbines perpendicular to the wind direction. In Layout 2, turbines extract energy from the wind at the front of the field and create wakes; the wind speed picks up again before the back row of turbines. Layout 1 is modeled after Middelgrunden Wind Farm [88]; designing single

rows of turbines for locations with a single dominant wind direction can help to drive down costs and increase power production.

Layout 2 also performed well for Case 2; this was unexpected, since at wind directions at 90 and 270 degrees, both of the rows are completely in the wake of upstream turbines. However, wake effects are minimal at the majority of wind directions. Layout 8 is modeled after Horns Rev wind farm and performs best in Case 2 [89]. Layout 8 has larger spacing than the other grid-like layout, Layout 9, and also has a slight offset.

The notable difference between the objective evaluations in Case 2 for Layouts 6 and 7 was unexpected. Both layouts contain the same number of turbines and the same square shape. However, their orientation and spacing are different. Turbines in Layout 7 are spread further apart than in Layout 6. The large difference in objective evaluations further suggests that the spacing and orientation of layouts plays a pivotal role in the overall power production. Wind data at potential offshore wind farm locations will vary based on geographic location; orienting the layout to maximize energy production greatly relies on knowledge of wind characteristics at a given location.

While the cost of transmission cabling is no small factor, it did not affect the best-performing layouts. Optimal spacing of turbines can reduce the cost of transmission cabling thus reducing the overall investment costs; however, optimizing layouts to increase power production is more important for the profitability of an offshore wind farm over its lifetime.

Chapter 9: Seeded Initial Layout Study Results and Discussion

9.1 Results

For the 4000 meter by 4000 meter area case, layouts were optimized for farms containing 16-52 turbines. The objective evaluations for farms optimized using seeded initial layouts are plotted in Fig. 25. For comparison, objective evaluations for layouts optimized using random initial layouts are plotted in Fig. 26.

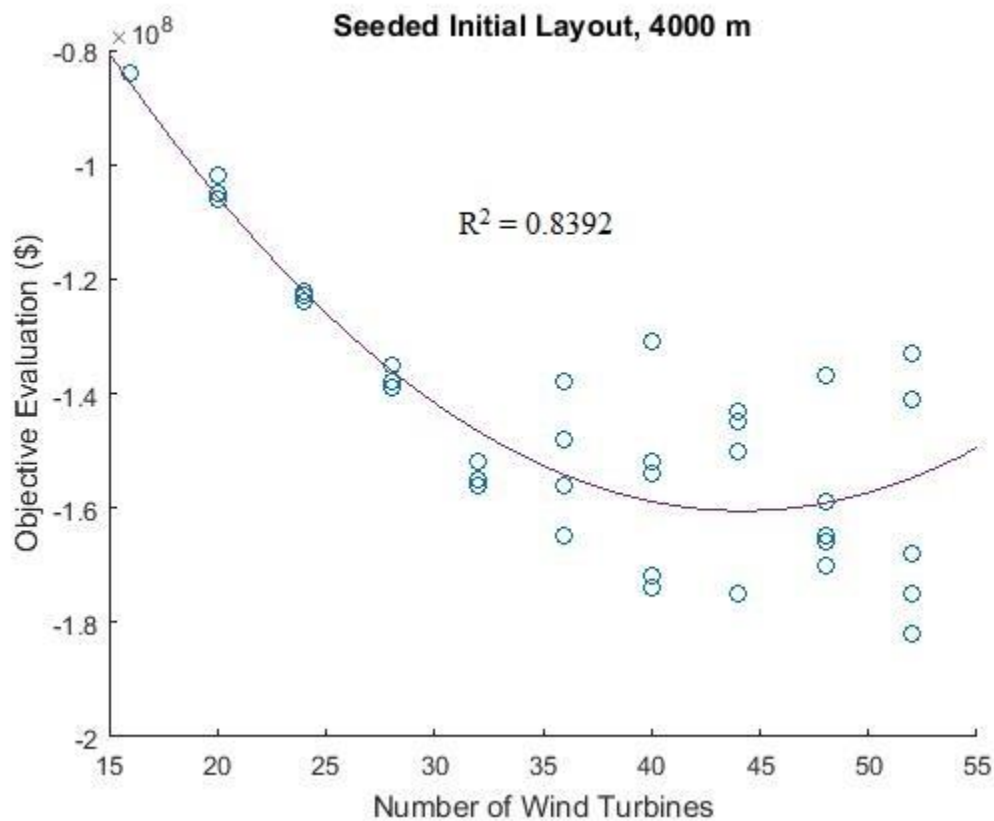


Fig. 25: Objective evaluations for 4000 meter optimized farms containing 16-52 turbines, seeded initial layouts

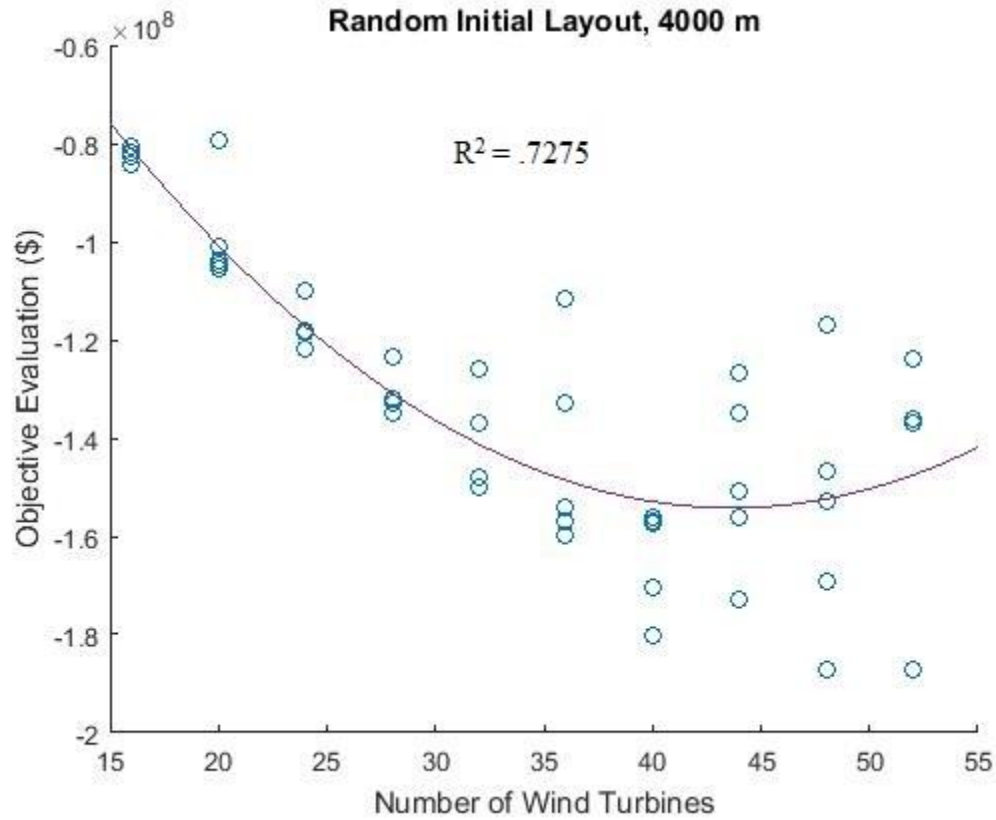


Fig. 26: Objective evaluations for 4000 meter optimized farms containing 16-52 turbines, random initial layouts

For the 2000 meter by 2000 meter area case, layouts were optimized for farms containing 4 - 48 turbines. The objective evaluations for farms optimized using seeded initial layouts are plotted in Fig. 27 ($R^2 = 0.8625$). For comparison, objective evaluations for layouts optimized using random initial layouts are plotted in Fig. 28 ($R^2 = 0.8197$).

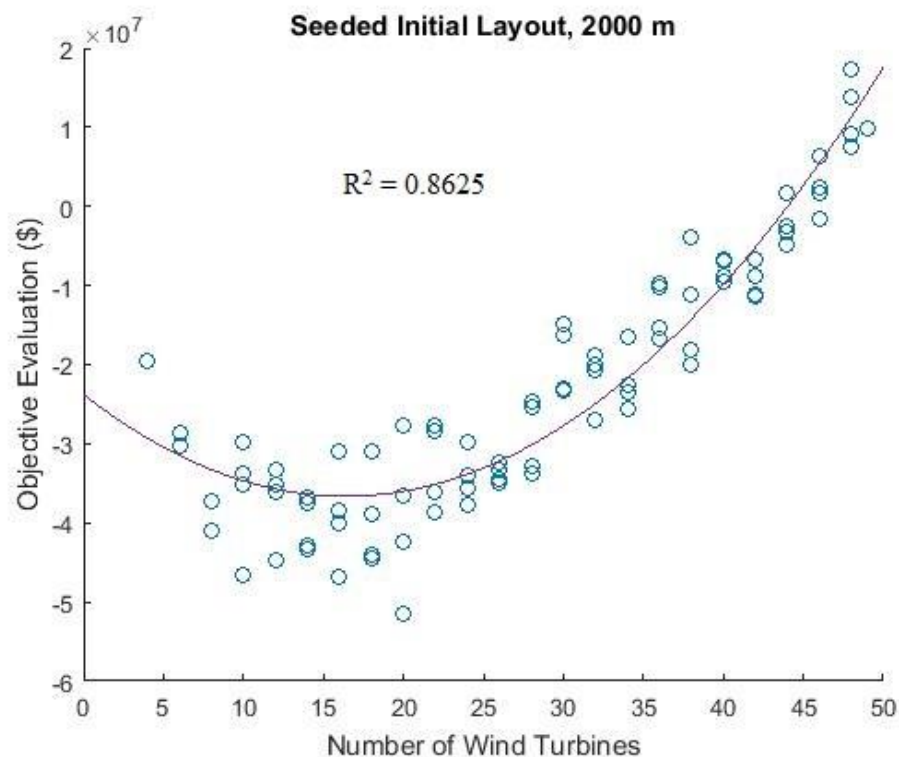


Fig. 27: Objective evaluations for 2000 meter optimized farms containing 4 – 48 turbines, seeded initial layouts

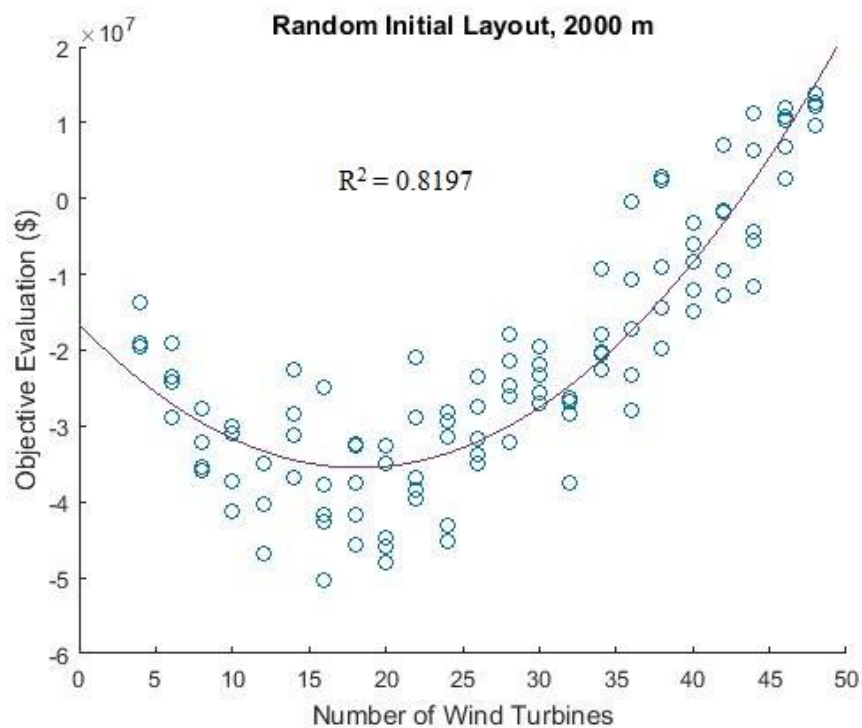


Fig. 28: Objective evaluations for 2000 meter optimized farms containing 4 – 48 turbines, random initial layouts

Optimal layouts for the seeded initial layout cases for both 4000 meter and 2000 meter wind farms are given in Figs. 29 and 30, respectively. The 4000 meter, 44 turbine layout has an objective evaluation of $-\$1.74\text{E}+08$. The 2000 meter, 20 turbine layout has an objective evaluation of $-\$5.25\text{E}+07$.

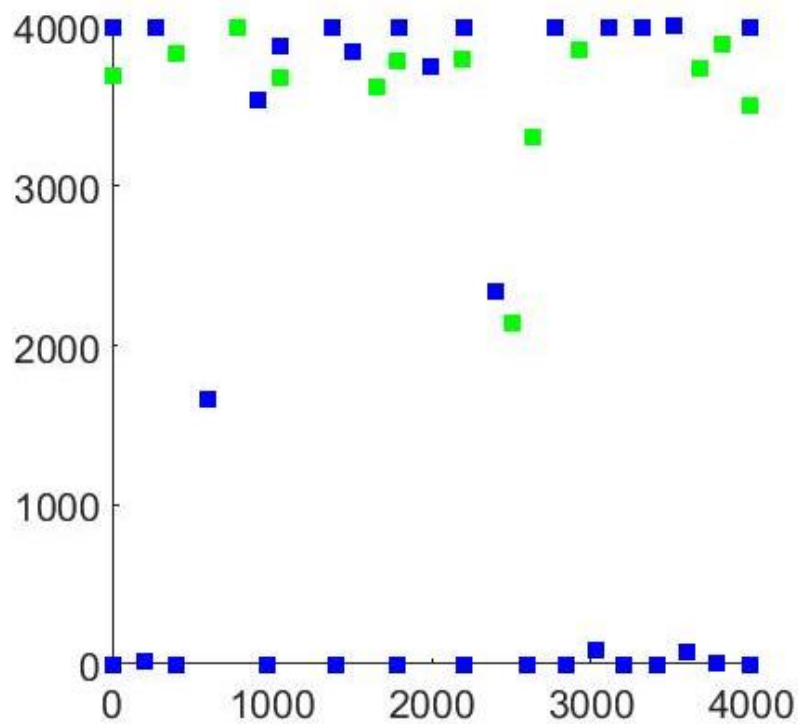


Fig. 29: 44 turbine, 4000 meter layout from seeded initial layout case; objective evaluation = $-\$1.74\text{E}+08$

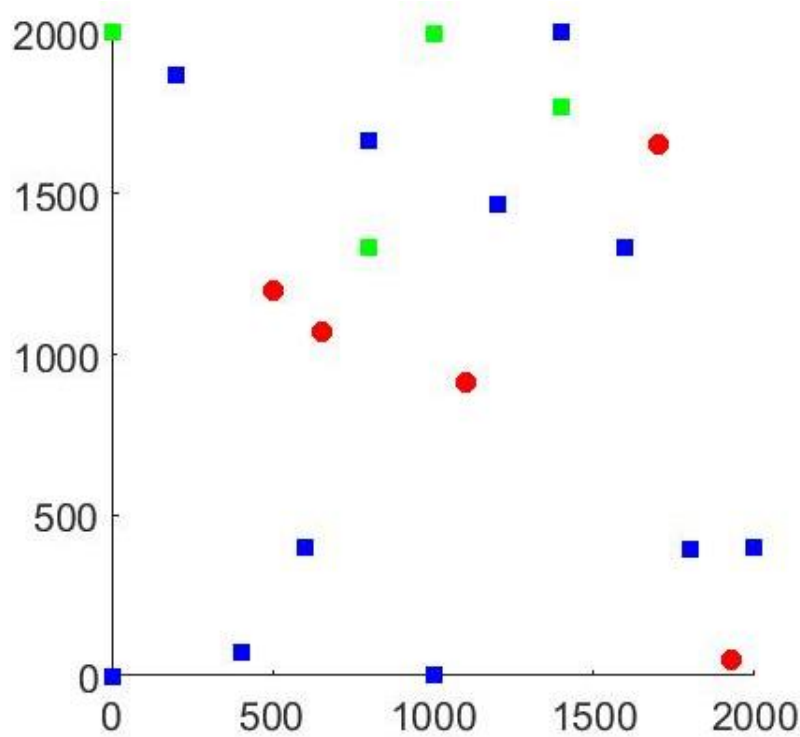


Fig. 30: 20 turbines, 2000 meter layout from seeded initial layout case; objective evaluation = $-\$5.25\text{E}+07$

9.2 Discussion

The minimum of the quadratic fit applied to the 4000-meter seeded initial layout (Fig. 25) occurs at 44 turbines (Fig. 29); the minimum objective evaluation is $-\$1.74\text{E}+08$. The minimum of the quadratic fit applied to the 4000-meter random initial layout (Fig. 26) also occurs at 44 turbines; the minimum objective evaluation is $-\$1.56\text{E}+08$. The inclusion of the seeded initial layouts did not affect the optimal number of turbines for the 4000-meter farm; however, the inclusion of the seeded initial layouts did decrease the minimum objective evaluation.

For the 2000-meter seeded initial layout case (Fig. 27), the minimum of the quadratic fit occurs at 20 turbines, and the minimum objective evaluation is $-\$5.25\text{E}+07$ (Fig. 30). The minimum of the fit for the random initial layout scenario (Fig. 28) occurs at 18 turbines, and the minimum objective evaluation is $-\$4.57\text{E}+07$. The inclusion of the seeded initial layouts decreased the minimum objective evaluation; in addition, it changed the optimal number of wind turbines in the farm.

Based on the comparisons between Figs. 25 and 26, and Figs. 27 and 28, it can be concluded that the inclusion of seeded layouts decreases noise in the fit of the objective evaluations. However, reduced noise in the data leading to a better fit created by the seeded layouts for the 4000 meter case is much greater than for the 2000 meter case. A square wind farm with 4000 meter side lengths has four times the area of a wind farm with 2000 meter side lengths. Since the EPS optimizes in a continuous space within the wind farm, the increase in area adds greatly to the number of solutions available. Therefore, it can be concluded that the inclusion of seeded initial layouts has a more positive impact on the fit of the data when the wind farm area is larger.

Chapter 10: Conclusions

In order to decrease the consumption of fossil fuels, reduce greenhouse gas emissions, and meet renewable portfolio standards, new renewable energy sources must be developed and implemented. Currently, floating offshore wind farms have very high costs that make them non-competitive as compared to other more established energy sources, such as onshore wind, solar, and fossil fuels. The purpose of this work was to discover optimal floating offshore wind farm layouts and turbine geometries and their corresponding profit objectives. Results can inform wind farm developers of expected power production and costs. Additionally, implementation of the presented optimized layouts will increase the overall profitability of floating offshore wind energy systems.

In the unidirectional wind case study discussed in Chapter 6, an EPS was applied to the optimization of floating offshore wind farm layouts in unidirectional, single wind speed conditions. Results from the offshore wind farm layouts were compared to similarly-optimized onshore wind farm layouts. It was discovered that comparable objective evaluations can be achieved for both the onshore and offshore layouts for farms containing a different number of turbines. While investment costs for offshore wind farms are much higher than onshore wind farms, over a life of 20 years they can achieve comparable profitability given the current problem formulation and modeling. In addition, while increasing the size of wind turbines increases investment costs, the offshore layouts chose to implement large turbine sizes, indicating that the power produced over the life of the farm will offset higher investment costs.

The EPS was also compared to resulting layouts obtained using an Adapted GA. For 16-turbine layouts, both the EPS and Adapted GA generated 100% efficient layouts. The EPS also generated 100% efficient layouts for farms containing twice as many turbines as the layout presented by the Adapted GA. It can be concluded that, for the simple wind case, the EPS is able to successfully optimize floating offshore wind systems in order to increase profitability.

In Chapter 7, an EPS method for optimizing offshore floating wind energy systems in multidirectional, multiple wind speed cases was presented. Turbine layout and geometry were optimized for 2000-meter square wind farms containing one to 22 turbines. Resulting layouts biased toward dominant wind directions; turbines were placed in rows perpendicular to the dominant wind directions, and along the perimeter of the field. A cubic fit with an R^2 value of 0.9026 was applied to the relationship between the number of turbines and the objective evaluations. The minimum occurred for wind farms containing five wind turbines. The overall minimum of the data presented was found for a seven turbine wind farm; over a life of 20 years, the seven turbine wind farm is expected to earn \$12 million dollars, and have an average energy production of 28.7 MW. The inclusion of the turbine geometry selection model increased the optimality of resulting layouts.

In Chapter 8, a study was presented that analyzed the profitability of hard-coded floating offshore wind farm layouts consisting of 3.6 MW wind turbines. For the system parameters presented, and at wind farm sites with a single dominant wind direction, floating wind turbines oriented in straight lines perpendicular to the dominant wind direction were shown to be ideal. Wind farm layouts with multiple dominant wind directions and wind speeds should be designed such that wake interactions are minimized at dominant wind directions. In addition, increased spacing between turbines will minimize wake interactions and optimize cost and power production. As wind turbine designs and the wind market changes, future work using advanced and state-of-the-art modeling will continue to provide offshore wind farm developers valuable information on best practices for optimally designing offshore wind farm layouts.

The study presented in Chapter 9 explored the effect of seeded initial layouts on the EPS's ability to consistently find good layouts. For the 4000-meter layouts, the inclusion of seeded initial layouts improved the R^2 value from 0.7275 to 0.8392, a 15.35% increase in fit. For the 2000-meter layouts, the inclusion of seeded initial layouts improved the R^2 value from 0.8197 to 0.8625, a 5.2% increase in fit. While farms of both sizes experienced an increased fit with the inclusion of seeded initial layouts, the larger farm experienced a greater increase. It can be concluded that the

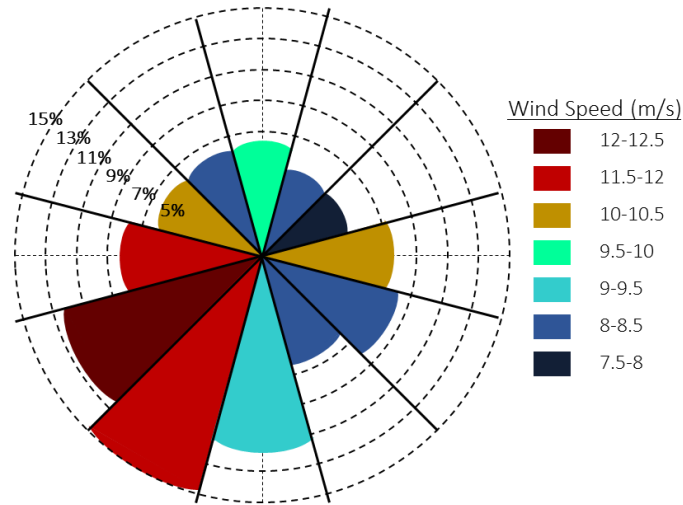
inclusion of seeded initial layouts increases the fit of the data more as the farm size is increased. For both the seeded and random initial layouts for the 4000-meter case, the minimum objective evaluation occurred at 44 turbines (-\$1.56E+08 random; -\$1.74E+08 seeded); however, for the 2000 meter case, the minimum occurred at 18 turbines for the random initial layout (-\$4.57E+07), and 20 turbines for the seeded initial layout (-\$5.15E+07). The minimum objective evaluations at the optimal number of turbines for all four farms was better in both seeded cases; it can be concluded that the inclusion of seeded initial layouts improved the overall objective evaluations. It is recommended that EPS algorithms applied to floating offshore wind farm systems optimization should include seeded initial layouts. While this decreases the stochasticity of the algorithm, it increases the ability of the EPS to consistently find better objective evaluations.

The work presented covered the optimization of floating offshore wind energy systems for many different scenarios. For wind sites with a single dominant wind speed and direction, the results presented in Chapter 6 can be used to inform developers of how to design optimal layouts. Similarly, Chapter 7 presents layouts that developers can use in designing floating offshore wind farms for wind sites with many wind speeds and directions. The work presented in Chapter 8 suggests optimal wind farms for developers who wish to implement layouts that are more uniform and symmetrical. Lastly, the exploratory work presented in Chapter 9 shows that using seeded initial layouts increases the fit of layouts discovered by the EPS for a unidirectional wind case.

Chapter 11: Future Work

11.1 Additional Studies

Realistic wind cases resemble the wind rose presented in Section 5.2 (Fig. 7), therefore, in order to inform developers of optimal wind farm layouts in real wind farms, further research must be conducted using the EPS to optimize wind systems in realistic, multidirectional wind cases. One study will compare results of the EPS to layouts generated using a Covariance Matrix Adaptation Evolutionary Strategy (CMA-ES) in a nested configuration presented by Rodrigues et al. [33]. This study optimized floating offshore wind farm layouts comprised of IDEOL floating platforms supporting 5 MW wind turbines [33,34]. The wind speeds and percentages of occurrence for each wind direction are given in Fig. 31.



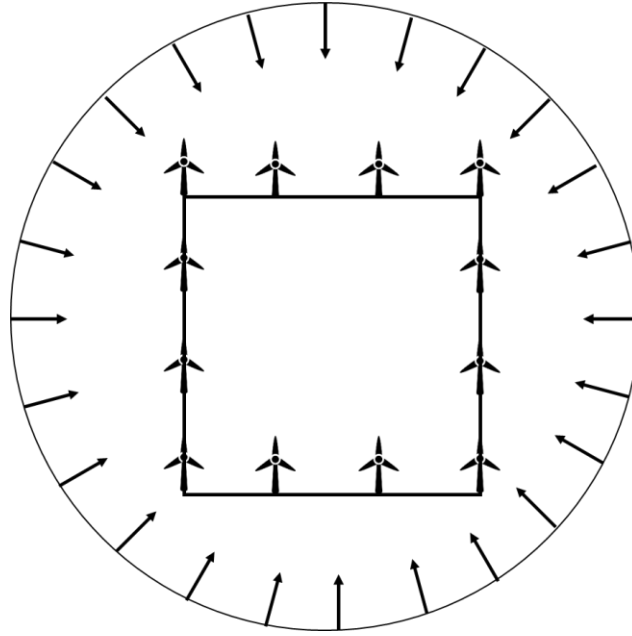


Fig 32: Seeded initial layout for multidirectional, multiple wind speed case.

11.2 Co-Located Array Optimization

Some research has begun to focus on locating wave energy converter (WEC) arrays with offshore wind farms. The models developed for this work were applied to a multi-objective GA to optimize the placement of co-located floating offshore wind turbines and WEC point absorbers.

11.3 Optimizing Cabling

Section 3.3.3 gives the cost of transmission cabling for an offshore wind farm. For inter-array cabling (the cabling used within a wind farm to connect all wind turbines to the export cable), the cost per kilometer is \$307,000 [73]. This cost can quickly become one of the most expensive elements of an offshore wind farm. Currently, the optimization methods presented in this work only account for turbine geometry and placement of turbines based on wake interactions. However, including spacing between turbines to account for the inter-array cabling costs will give more accurate objective evaluations for real wind farms. This may be achieved by including a Traveling Salesman sub-optimization within the EPS.

References

- [1] Martin, L., 2014, “Lower U.S. electricity demand growth would reduce fossil fuels’ projected generation share,” EIA.
- [2] Archer, C. L., 2005, “Evaluation of global wind power,” *J. Geophys. Res.*, **110**(D12), p. D12110.
- [3] EWEA, 2015, “The European offshore wind industry key 2015 trends and statistics,” ... — Doc. ..., (January), p. 31.
- [4] Lindenberg, S., Smith, B., and O’Dell, K., 2008, 20% Wind energy by 2030, Washington, DC.
- [5] Schwartz, M., Heimiller, D., Haymes, S., and Musial, W., 2010, Assessment of Offshore Wind Energy Resources for the United States, Golden, Colorado.
- [6] Breton, S. P., and Moe, G., 2009, “Status, plans and technologies for offshore wind turbines in Europe and North America,” *Renew. Energy*.
- [7] Sclavounos, P. D., Tracy, C., and Lee, S., 2007, “Floating Offshore Wind Turbines: Responses in a Seastate, Pareto Optimal Designs and Economic Assessment,” *Int. Conf. Offshore ...*, pp. 1–20.
- [8] Sclavounos, P., 2008, “Floating Offshore Wind Turbines,” *Mar. Technol. Soc. J.*, **42**(2), pp. 39–43.
- [9] Lawson, J., 2013, “Good foundations : the pros and cons of monopiles,” *WorldWind Technol.*, (December).
- [10] Byrne, B. W., and Houlsby, G. T., 2003, “Foundations for offshore wind turbines,” *Philos. Trans. A. Math. Phys. Eng. Sci.*
- [11] Roddier, D., Cermelli, C., Aubault, A., and Weinstein, A., 2010, “WindFloat: A floating foundation for offshore wind turbines,” *J. Renew. Sustain. Energy*, **2**, pp. 1–34.
- [12] Carrington, D., 2014, “Drifting off the coast of Portugal, the frontrunner in the global race for floating wind farms,” *Guard*.
- [13] 2014, “Marine Transmission in Oregon Oregon Department of Energy Marine Transmission in Oregon Marine Transmission in Oregon Report to Oregon Legislature.”
- [14] Principle Power, 2014, “U.S. Department of Energy Supports Oregon Offshore Wind with Grant Accelerating Development of WindFloat Pacific Project,” p. Press Release.
- [15] Mosetti, G., Poloni, C., and Diviacco, B., 1994, “Optimization of wind turbine positioning in large windfarms by means of a genetic algorithm,” *J. Wind Eng. Ind. Aerodyn.*, **51**(1), pp. 105–116.
- [16] DuPont, B., Cagan, J., and Moriarty, P., 2015, “AN ADVANCED MODELING SYSTEM FOR OPTIMIZATION OF WIND FARM LAYOUT

AND WIND TURBINE SIZING USING A MULTI-LEVEL EXTENDED,”
Energy, **In Press**, pp. 1–26.

- [17] DuPont, B. L., and Cagan, J., 2012, “An Extended Pattern Search Approach to Wind Farm Layout Optimization,” *ASME J. Mech. Des.*, **134**, pp. 1–18.
- [18] DuPont, B. L., and Cagan, J., 2013, “Multi-Stage Optimization of Wind Farms with Limiting Factors,” *ASME Int. Des. Eng. Tech. Conf. Comput. Inf. Eng. Conf.*, pp. 1–12.
- [19] DuPont, B. L., Cagan, J., and Moriarty, P., 2012, “Optimization of Wind Farm Layout and Wind Turbine Geometry Using a Multi-Level Extended Pattern Search Algorithm That Accounts for Variation in Wind Shear Profile Shape,” Volume 3: 38th Design Automation Conference, Parts A and B, Chicago, Illinois, USA, p. 243.
- [20] Ozturk, U. A., and Norman, B. a., 2004, “Heuristic methods for wind energy conversion system positioning,” *Electr. Power Syst. Res.*, **70**(3), pp. 179–185.
- [21] Wan, C., Wang, J., Yang, G., and Zhang, X., 2010, “Particle swarm optimization based on Gaussian mutation and its application to wind farm micro-siting,” *49th IEEE Conf. Decis. Control*, (2), pp. 2227–2232.
- [22] Pookpunt, S., and Ongsakul, W., 2013, “Optimal placement of wind turbines within wind farm using binary particle swarm optimization with time-varying acceleration coefficients,” *Renew. Energy*, **55**, pp. 266–276.
- [23] Elkinton, C. N., Manwell, J. F., and McGowan, J. G., 2005, “Offshore Wind Farm Layout Optimization (OWFLO) Project: An Introduction,” *Optimization*.
- [24] Elkinton, C. N., Manwell, J. F., and McGowan, J. G., 2008, “Algorithms for Offshore Wind Farm Layout,” *Wind Eng.*, **32**(1), pp. 67–83.
- [25] Pérez, B., Mínguez, R., and Guanche, R., 2013, “Offshore wind farm layout optimization using mathematical programming techniques,” *Renew. Energy*.
- [26] Gao, X., Yang, H., and Lu, L., 2014, “Investigation into the optimal wind turbine layout patterns for a Hong Kong offshore wind farm,” *Energy*, **73**(June 2015), pp. 430–442.
- [27] Gao, X., Yang, H., Lin, L., and Koo, P., 2015, “Wind turbine layout optimization using multi-population genetic algorithm and a case study in Hong Kong offshore,” *J. Wind Eng. Ind. Aerodyn.*, **139**, pp. 89–99.
- [28] Réthoré, P. E., Fuglsang, P., Larsen, G. C., Buhl, T., Larsen, T. J., and Madsen, H. a., 2013, “TOPFARM: Multi-fidelity optimization of offshore wind farms,” *Wind Energy*, (DECEMBER).
- [29] Liu, F., and Wang, Z., 2014, “Offshore Wind Farm Layout Optimization Using Adapted Genetic Algorithm: A different perspective.”
- [30] Rivas, R. A., Clausen, J., Hansen, K. S., and Jensen, L. E., 2009, “Solving the Turbine Positioning Problem for Large Offshore Wind Farms by Simulated

- Annealing,” *Wind Eng.*, **33**(3), pp. 287–297.
- [31] Salcedo-Sanz, S., Gallo-Marazuela, D., Pastor-Sánchez, A., Carro-Calvo, L., Portilla-Figueras, A., and Prieto, L., 2014, “Offshore wind farm design with the Coral Reefs Optimization algorithm,” *Renew. Energy*.
 - [32] Ituarte-Villarreal, C. M., and Espiritu, J. F., 2011, “Optimization of wind turbine placement using a viral based optimization algorithm,” *Procedia Comput. Sci.*, **6**, pp. 469–474.
 - [33] Rodrigues, S. F., Teixeira Pinto, R., Soleimanzadeh, M., Bosman, P. a. N., and Bauer, P., 2015, “Wake losses optimization of offshore wind farms with moveable floating wind turbines,” *Energy Convers. Manag.*, **89**, pp. 933–941.
 - [34] Guérivière, P. de la, 2011, Press Release: IDEOL Announces a New Floating Platform Solution to Accelerate the Deployment of Offshore Wind Farms, La Ciotat, France.
 - [35] Torczon, V., 1997, “On the convergence of pattern search algorithms,” *SIAM J. Optim.*, **7**(1), pp. 1–25.
 - [36] Torczon, V., and Trosset, M. W., 1997, “From Evolutionary Operation to Parallel Direct Search : Pattern Search Algorithms for Numerical Optimization,” *Comput. Sci. Stat.*, **29**(1), pp. 396–401.
 - [37] Aladahalli, C., Cagan, J., and Shimada, K., 2007, “Objective Function Effect Based Pattern Search—Theoretical Framework Inspired by 3D Component Layout,” *J. Mech. Des.*, **129**(3), p. 243.
 - [38] Yin, S., and Cagan, J., 2004, “Exploring the Effectiveness of Various Patterns in an Extended Pattern Search Layout Algorithm,” *J. Mech. Des.*, **126**(1), p. 22.
 - [39] Vaz, A. I. F., and Vicente, L. N., 2007, “A particle swarm pattern search method for bound constrained global optimization,” *J. Glob. Optim.*, **39**(2), pp. 197–219.
 - [40] Cagan, J., 2000, “A Survey of Computational Approaches to Three-dimensional Layout Problems,” *Comput. Aided Des.*, (412), pp. 1–33.
 - [41] Rajper, S., and Amin, I. J., 2012, “Optimization of wind turbine micrositeing: A comparative study,” *Renew. Sustain. Energy Rev.*, **16**(8), pp. 5485–5492.
 - [42] Elkinton, C. N., Manwell, J. F., and McGowan, J. G., 2009, “Algorithms for Offshore Wind Farm Layout Optimization,” *Wind Eng.*, **32**(1), pp. 67–84.
 - [43] Fuglsang, P., and Thomsen, K., 1998, Cost Optimization of Wind Turbines for Large-scale Off-shore Wind Farms.
 - [44] Butterfield, S., Jonkman, J., and Sclavounos, P. P., 1990, “Engineering Challenges for Floating Offshore Wind Turbines By.”
 - [45] Bresesti, P., Kling, W. L., Hendriks, R. L., and Vailati, R., 2007, “HVDC connection of offshore wind farms to the transmission system,” *IEEE Trans.*

Energy Convers., **22**(1), pp. 37–43.

- [46] Castro-Santos, L., Ferreño González, S., and Diaz-Casas, V., 2013, “Methodology to calculate mooring and anchoring costs of floating offshore wind devices,” International Conference on Renewable Energies and Power Quality (ICRE PQ)1, Bilbao.
- [47] Bussel, G. J. W. W. Van, Zaaier, M. B. B., and Sc, M., 2001, “Reliability , Availability and Maintenance aspects of large-scale offshore wind farms , a concepts study,” MAREC 2001 Mar. Renew. Energies Conf., **113**, pp. 119–126.
- [48] 2009, “Hywind Demo” [Online]. Available: <http://www.statoil.com/>.
- [49] Henderson, a R., Zaaier, M. B., Bulder, B., Pierik, J., Huijsmans, R., Van Hees, M., Snijders, E., Wijnants, G. H., and Wolf, M. J., 2004, “Floating windfarms for shallow offshore sites,” Proc. 14th Int. Offshore Polar Eng. Conf., pp. 120–127.
- [50] Barthelmie, R. J., Pryor, S. C., Frandsen, S. T., Hansen, K. S., Schepers, J. G., Rados, K., Schlez, W., Neubert, a., Jensen, L. E., and Neckelmann, S., 2010, “Quantifying the impact of wind turbine wakes on power output at offshore wind farms,” J. Atmos. Ocean. Technol., **27**(8), pp. 1302–1317.
- [51] Barthelmie, R. J., Frandsen, S., Rathmann, O., and K, 2008, “Flow and wakes in large wind farms in complex terrain and offshore,” Eur. Wind Energy, p. 10.
- [52] Kusiak, A., Zheng, H., and Song, Z., 2009, “Wind farm power prediction: a data-mining approach,” Wind Energy, **12**(3), pp. 275–293.
- [53] Jensen, N. O., 1983, “A Note on wind generator interaction,” Risø-M, p. 16.
- [54] Du Pont, B. L., and Cagan, J., 2012, “An Extended Pattern Search Approach to Wind Farm Layout Optimization,” J. Mech. Des., **134**(August 2012), p. 081002.
- [55] De Prada Gil, M., Gomis-Bellmunt, O., Sumper, A., and Bergas-Jané, J., 2012, “Power generation efficiency analysis of offshore wind farms connected to a SLPC (single large power converter) operated with variable frequencies considering wake effects,” Energy, **37**(1), pp. 455–468.
- [56] Ainslie, J. F., 1988, “Calculating the flowfield in the wake of wind turbines,” J. Wind Eng. Ind. Aerodyn., **27**(1-3), pp. 213–224.
- [57] Barthelmie, R. J., Hansen, K., Frandsen, S. T., Rathmann, O., Schepers, J. G., Schlez, W., Phillips, J., Rados, K., Zervos, a., Politis, E. S., and Chaviaropoulos, P. K., 2009, “Modelling and measuring flow and wind turbine wakes in large wind farms offshore,” Wind Energy, **12**(5), pp. 431–444.
- [58] Lange, B., Waldl, H. P., Guerrero, A. G., Heinemann, D., and Barthelmie, R. J., 2003, “Modelling of offshore wind turbine wakes with the wind farm program FLaP,” Wind Energy, **6**(1), pp. 87–104.

- [59] Martínez, D. C., 2013, “Development of a wake model for wind farms based on an open source CFD solver . Strategies on parabolization and turbulence modeling,” Universidad Politécnica de Madrid.
- [60] Kusiak, A., and Song, Z., 2010, “Design of wind farm layout for maximum wind energy capture,” *Renew. Energy*, **35**(3), pp. 685–694.
- [61] Sørensen, P., Cutululis, N. A., Viguera-Rodríguez, A., Madsen, H., Pinson, P., Jensen, L. E., Hjerrild, J., and Donovan, M., 2008, “Modelling of power fluctuations from large offshore wind farms,” *Wind Energy*, **11**(1), pp. 29–43.
- [62] Larsen, G. C., 2007, Dynamic wake meandering modeling.
- [63] Özdemir, H., Versteeg, M. C., and Brand, A. J., 2013, “Improvements in ECN Wake Model,” ICOWES2013 Conf. Lyngby, Denmark, (August), pp. 17–19.
- [64] Bot, E. T. G., 2012, Farmflow – improved near wake modelling and validation against four full scale wind farms.
- [65] Andersen, S. J., Sørensen, J. N., Ivanell, S., and Mikkelsen, R. F., 2014, “Comparison of Engineering Wake Models with CFD Simulations,” *J. Phys. Conf. Ser.*, **524**(1), p. 012161.
- [66] Jasak, H., Jemcov, A., and Tukovic, Z., 2007, “OpenFOAM: A C++ Library for Complex Physics Simulations,” *Int. Work. Coupled Methods Numer. Dyn.*, **m**, pp. 1–20.
- [67] Barthelmie, R. J., Badger, J., Pryor, S. C., Hasager, C. B., Christiansen, M. B., and Jørgensen, B. H., 2009, “Offshore Coastal Wind Speed Gradients: issues for the design and development of large offshore windfarms,” *Wind Eng.*, **31**(6), pp. 369–382.
- [68] Manwell, J. F., McGowan, J. G., and Rogers, A. L., 2009, *Wind Energy Explained: theory, design, and application*, John Wiley & Sons Ltd., West Sussex, UK.
- [69] Hegberg, T., Corten, G. P., and Eecen, P. J., 2004, “Turbine Interaction in Large Offshore Wind Farms,” *Ecnnl*, (August).
- [70] Chowdhury, S., Zhang, J., Messac, A., and Castillo, L., 2012, “Unrestricted wind farm layout optimization (UWFLO): Investigating key factors influencing the maximum power generation,” *Renew. Energy*, **38**(1), pp. 16–30.
- [71] Jonkman, J., Butterfield, S., Musial, W., and Scott, G., 2009, “Definition of a 5-MW reference wind turbine for offshore system development,” *Contract*, (February), pp. 1–75.
- [72] Castro-Santos, L., and Diaz-Casas, V., 2014, “Life-cycle cost analysis of floating offshore wind farms,” *Renew. Energy*, **66**, pp. 41–48.
- [73] Myhr, A., Bjerkseter, C., Ågotnes, A., and Nygaard, T. a., 2014, “Levelised cost of energy for offshore floating wind turbines in a life cycle perspective,”

- Renew. Energy, **66**, pp. 714–728.
- [74] Castro-Santos, L., and Diaz-Casas, V., 2015, “Economic influence of location in floating offshore wind farms,” *Ocean Eng.*, **107**, pp. 13–22.
 - [75] 2011, “WindFloat” [Online]. Available: www.principlepowerinc.com.
 - [76] Lantz, E., Goldberg, M., and Keyser, D., 2013, “Jobs and Economic Development Impact (JEDI) Model: Offshore Wind User Reference Guide,” (June).
 - [77] Baker, C., 2015, “Substation Costs.”
 - [78] 2015, “Bureau of Ocean Energy Management,” Dep. Energy.
 - [79] 2012, Commercial Lease of Submerged Lands for Renewable Energy Development on the Outer Continental Shelf, Herndon, VA.
 - [80] Hooke, R., and Jeeves, T. A., 1961, ““Direct Search” Solution of Numerical and Statistical Problems,” *J. ACM*, **8**(2), pp. 212–229.
 - [81] Torczon, V., 1995, “Pattern Search Methods for Nonlinear Optimization,” *SIAG/OPT Views News*, **6**, pp. 7–11.
 - [82] Yin, S., and Cagan, J., 2000, “An Extended Pattern Search Algorithm for 3D Component Layout.”
 - [83] Hsu, S. a., Meindl, E. a., and Gilhousen, D. B., 1994, “Determining the power-law wind-profile exponent under near-neutral stability conditions at sea,” *Am. Meteorol. Soc.*, pp. 757–765.
 - [84] Siemens, 2010, “SWT-3.6-107 Wind Turbine.”
 - [85] Foster, G., and Ferguson, S., 2013, “Enhanced Targeted Initial Populations for Multiobjective Product Line Optimization,” *International Design Technical Conferences & Computers and Information in Engineering Conference*, Portland, OR, pp. 1–13.
 - [86] Foster, G., Turner, C., Ferguson, S., and Donndelinger, J., 2014, “Creating targeted initial populations for genetic product searches in heterogeneous markets,” *Eng. Optim.*, **46**(12), pp. 1729–1747.
 - [87] Maaranen, H., Miettinen, K., and Penttinen, A., 2007, On initial populations of a genetic algorithm for continuous optimization problems.
 - [88] Barthelmie, R. J., Frandsen, S. T., Nielsen, M. N., Pryor, S. C., Rethore, P. E., and Jørgensen, H. E., 2007, “Modelling and measurements of power losses and turbulence intensity in wind turbine wakes at middelgrunden offshore wind farm,” *Wind Energy*, **10**(6), pp. 517–528.
 - [89] Méchali, M., Barthelmie, R., Frandsen, S., Jensen, L., and Réthoré, P.-E., 2006, “Wake effects at Horns Rev and their influence on energy production,” *Eur. Wind Energy Conf. Exhib.*, (1), pp. 10–20.